Climatological study on atmospheric water cycling over the Maritime Continent

（海洋大陸上における大気水循環の気候学的研究）

Hironari Kanamori

（金森　大成）

Doctor of Science

Graduate School of Environmental Studies, Nagoya University

（名古屋大学大学院環境学研究科　博士（理学））

2015

Abstract

This study investigates spatiotemporal characteristics of the diurnal cycle of precipitation over Sarawak in northwest Borneo, associated with large-scale intraseasonal disturbances represented by the Madden–Julian Oscillation (MJO). The atmospheric water cycles are investigated over several timescales to understand the maintenance processes that control heavy precipitation over the islands of the Maritime Continent.

The detail behavior of the diurnal cycle of precipitation is accomplished using a combination of data from a dense hourly rain gauge network and satellites. The spatial pattern of the diurnal cycle is classified into two major groups of coastal and interior regions based on distinct differences in precipitation peak times and amplitudes. Amplitudes of the DC and daily precipitation amount increase in active MJO phases at all sites, with a stronger effect evident in the coastal region compared with the interior region. This modulation of precipitation by the MJO disturbance is attributed to precipitation frequency in the interior region, and to both the frequency and intensity of precipitation in the coastal region. The low-level westerly wind anomaly enhances convergence, the land–sea breeze and a midnight precipitation peak in the coastal region during the active MJO phase. Results from the analysis of moisture flux divergence and moist static instability suggest these could be responsible for the different dynamics of this modulation of the diurnal cycle between coastal and interior regions.

On the other hand, large island regions can be divided into land, coastal, and ocean areas based on the characteristics of the hydrological cycle and diurnal variations in precipitation. Within the Maritime Continent, the major islands of Borneo and New Guinea exhibit different water cycles. Large-scale circulation variations, such as the seasonal cycle and the MJO, have a lesser effect on the hydrological cycle over Borneo than over New Guinea. However, the impact of diurnal cycle on regional-scale circulation and water exchange between land and coastal regions is pronounced over both islands. The local water use ratio is higher over Borneo than over New Guinea, which may be related to a stronger diurnal variation in the atmospheric water cycle that results from higher evapotranspiration over tropical rainforests.

Contents

List of tables

List of figures

1. Introduction

1.1. General features of the Maritime Continent

The Maritime Continent (MC) is an oceanic region in Southeast Asia that contains large islands such as New Guinea, Borneo, and Sumatra. This shallow ocean environment contains many islands and lies within a tropical warm pool (Ramage 1968). Major islands in the MC are characterized by heavy precipitation because the topography generates localized convection and leads to the formation of active cloud/precipitation systems (Neale and Slingo 2003; Biasutti et al. 2012; Peatman et al. 2014). Convective cloud systems in the MC release large amounts of latent heat and play a major role in the atmospheric heat budget. Thus, land–sea thermal contrasts associated with these major islands in the warm ocean environments generate complex local circulations that play an important role in the energy and water cycle of the MC (Neale and Slingo 2003). Much of the active deep convection occurs in response to the interactions among circulation systems across different temporal and spatial scales over and around the islands. The linkage between island-induced convection and the large-scale circulation is crucial for convective organization over this region.

Temporal variations in convection and precipitation exhibit a pronounced diurnal and intraseasonal variability, and large-scale processes such as the Madden–Julian oscillation (MJO) (Madden and Julian 1971, 1972, 1994) play a key role in intraseasonal variability over the MC (Ichikawa and Yasunari 2006, 2008; Rauniyar and

Walsh 2011). Heavy precipitation and deep convection are especially evident over Borneo, which is the large and most central island of the MC, and are strongly associated with large-scale tropical disturbances such as the MJO, the Borneo vortex, and cold surges during the boreal winter (Chang et al. 2005a).

1.2. Impact of the MJO on diurnal cycle of convection and precipitation

The MC also has a pronounced diurnal cycle (DC) of convection and precipitation associated with surface thermal contrasts between the islands and surrounding oceans. The DC of convection can develop into organized cloud systems given the very moist tropical atmosphere. Previous studies show a pronounced DC of convection with late afternoon-to-evening maxima over land, and night-to-morning maxima over the surrounding seas (Houze et al. 1981; Murakami 1983; Williams and Houze 1987; Nitta and Sekine 1994; Chen and Takahashi 1995; Ohsawa et al. 2001; Yang and Slingo 2001; Neale and Slingo 2003; Kikuchi and Wang 2008). In the boreal winter monsoon period, land breezes converge with northeasterly monsoons to generate offshore convection and heavy precipitation between midnight and morning over western Borneo (Houze et al. 1981).

Precipitation variability appears to be influenced by the seasonal cycles of the summer and winter monsoons, particularly over oceanic and coastal areas of the western MC (Chang et al. 2005g). However, the seasonal cycle of precipitation is relatively weak, especially over Borneo in the MC equatorial area (Kumagai et al. 2005). In this

area, the MJO is a remarkable feature of atmospheric circulation and moist convection that fundamentally modulates the heavy precipitation seen here (Madden and Julian 1994; Zhang 2005). Disturbances on the MJO mainly control the atmospheric heat source by releasing a significant amount of latent heat (Lin et al. 2004). Therefore, the interaction between the DC of precipitation (DCP) and the MJO is an important issue for both understanding local and regional precipitation processes, and assessing predictions regarding the global climate.

Previous studies have reported the impact of the MJO on the DC. For example, Chen and Takahashi (1995) examined the contrast in land–sea cumulus convection DC during the active/break phase of the MJO over the South China Sea using equivalent blackbody temperature from a geostationary meteorological satellite (GMS) and found that the DC of convection is suppressed in the MJO active phase over the MC. A similar result was reported using GMS and radar reflectivity as part of the Tropical Ocean Global Atmosphere Coupled Ocean Atmosphere Response Experiment (TOGA COARE) conducted in the western Pacific (Sui and Lau 1992; Sui et al. 1997). However, an analysis of the Tropical Rainfall Measuring Mission (TRMM) 3B42 product merged with infrared (IR) radiation data suggests the opposite (Tian et al. 2006). Using TRMM 3B42 and 3G68 datasets, Rauniyar and Walsh (2011) showed that precipitation rates are enhanced over the ocean during active MJO days, while precipitation rates over the islands are enhanced during suppressed MJO days. Ichikawa and Yasunari (2006) identified a different propagation feature over Borneo associated with large-scale circulation field changes related to MJO disturbances using TRMM

precipitation radar (PR) data. Thus, the effect of the MJO on the DC is still controversial.

The characteristics of the DC in relation to MJO active phases (with large-scale cloud disturbances) or break phases (without such disturbances) are a matter of keen interest, but the TRMM dataset cannot provide information on temporal evolution. One controversial but critical question is whether the DCP over the MC is affected solely by MJO disturbances. To address this issue I must be careful to use precipitation rates based on convection intensity, for example equivalent blackbody temperature or outgoing longwave radiation (OLR), because heavy precipitation frequently occurs from low-level stratiform clouds associated with cloud/precipitation systems over the major MC islands (e.g., Ichikawa and Yasunari 2006). In addition, it was suggested that the DCP, which is influenced by variations of large-scale, low-level circulations, differs from the coast to the island interior (Ichikawa and Yasunari 2006). Precipitation data from a dense ground-based network are advantageous in tackling this issue. Other precipitation indices, such as frequency and intensity of the precipitation rate DC, should be examined in addition to precipitation amounts to better describe the characteristics of the DC in this region.

Seasonal and interannual variability of precipitation based on rain gauge datasets has been identified in the Indonesian territory of the MC region (Hamada et al. 2002; Hamada et al. 2008), Borneo (Gomyo and Kuraji 2006), and the Malay Peninsula and Borneo (Oki and Musiake 1994; Ohsawa et al. 2001). Oki and Musiake (1994) also found a windward shift in coastal morning maxima of precipitation against the

predominant monsoon winds based on hourly rain gauge data along the shoreline. The effect of the MJO on the DCP over the MC has not been investigated because dense hourly rain gauge data from the coastal to the interior region of the island are required to do this.

1.3. Atmospheric water cycling over the Maritime Continent

Deep convection and heavy precipitation throughout the year create a major moisture sink in the MC. Atmospheric water budget analyses over the MC show that moisture flux convergence variability contributes to precipitation variability on the MJO timescale (Chen et al. 1995). In addition, Waliser et al. (2009) used satellite data to show that increasing (decreasing) precipitation is maintained by the preceding moisture flux convergence (divergence) on MJO timescales, and that the contribution of evaporation to precipitation is relatively small.

However, tropical rainforests are a major source of global and regional hydrologic fluxes (Aragao 2012) and evapotranspiration over land may also play a major role in hydrological cycles in the MC. For example, estimates from ground-based observations suggest that the contribution of evapotranspiration to annual precipitation in western Borneo ranges from about 50% (Kume et al. 2011) to 74% (Kumagai et al. 2005). However, a study based on a General Circulation Model (GCM) suggests that water recycling is not significant in Borneo (Goessling and Reick 2011), and Kumagai et al. (2013) showed that the climatological annual mean moisture flux convergence over Borneo made little contribution to precipitation totals despite heavy precipitation

throughout the year. Because the moisture flux convergence makes a large contribution to precipitation in other major islands such as New Guinea (Kumagai et al. 2013), it must be assumed that the hydrological cycle is different on each island. Furthermore, variations in forest cover may also significantly modify climatic and hydrological cycles at regional and global scales. Evapotranspiration from forests has the capacity to modify precipitation and, in turn, the regional water balance (Kanae et al. 2001; Yasunari et al. 2006; Bonan 2008; Spracklen et al. 2012). Therefore, water budget analyses must be conducted separately for complex land and ocean areas in the MC.

1.4. Purpose of the present study

This study examines temporal and spatial variations in diurnal rainfall over the MC. A particular question addressed is how the large-scale circulation field changes associated with a passage of MJO disturbance modulate the DCP over the islands and the adjacent oceans. Furthermore, this study focuses on how much precipitation over the islands is governed by the relationship between the atmospheric and surface conditions. Through detailed analysis of the atmospheric data sets the linkage between the diurnal cycle and the large-scale intraseasonal disturbance is investigated, together with the atmospheric water cycle over the MC. These topics not only reveal the climate of the regional scale over the MC, but are also important in the understanding of the global water cycle.

This study examines how the DCP is affected by MJO disturbances, along with its time–space characteristics over the ocean, coastal regions, and island interiors, with

particular reference to the major MC islands. This, in turn, should deal with the question as to how the original MJO cloud system from the Indian Ocean is modified through the DC over the major MC islands. I use a dense hourly rain gauge network across the Malaysian state of Sarawak in western Borneo together with TRMM data to address the various characteristics of interactions between the DC of land and ocean systems.

Also, to revel the heavy precipitation is maintained over the over the MC, this study estimates the atmospheric water budget over the MC. To provide a better understanding of the processes responsible for heavy precipitation in the hydrological cycle, this study estimates the land and ocean atmospheric water budget over the MC. Because the impact of large-scale circulations on the diurnal precipitation cycle differs between major islands in the MC, it is necessary to calculate the water budget separately for each island. This work focuses on New Guinea and Borneo, which are, respectively, the largest and the second largest islands in the region.

The remainder of this paper is organized as follows: Chapter 2 outlines the data used in this study and the methods of analysis. In Chapter 3, the modulation of the DCP associated with the MJO observed by a dense hourly rain gauge network over the western part of Borneo is described. Chapter 4 presents the effects of various timescales of atmospheric water cycles on the water balance over the MC. Chapter 6 discusses the overall feature of this study, and Chapter 7 presents the final conclusions.

2. Datasets and Methods of analysis

2.1. Daily and hourly rain gauge data

Daily and hourly precipitation data from 50 (almost uniformly distributed) rain stations in Sarawak, Malaysia, Borneo from 1999–2003 (5 years of data) were compiled by the Department of Irrigation and Drainage, Sarawak and the Malaysian Meteorological Department. These stations have precipitation datasets with hourly (19 stations) or daily (30 stations) temporal resolution. This study also used hourly rain gauges in Lambir Hills National Park (N.P.) (4°20′N, 113°50′E), which is about 12 km from the nearest coast. Figure 3.1b shows locations of both the daily and hourly precipitation stations. Table 3.1 shows more detailed information on the 20 hourly precipitation stations, which are at altitudes less than 1000 meters above sea level to the west of the Iran Mountains. To focus on the DC, I calculated 3-hourly running means at all stations. Times of maximum and minimum precipitation are directly derived from the DC of these data (Ohsawa et al. 2001). This study determined the hours of maximum and minimum precipitation that were more or less than the daily mean precipitation. I defined the largest maximum precipitation peak as a maximum peak. This method detected a semidiurnal cycle, with two maximum and two minimum precipitation peaks, at some stations. The larger maximum precipitation was called the first maximum precipitation peak and the other the secondary maximum precipitation peak. This work also defined the amplitude of the DCP as the difference in precipitation amount between the maximum precipitation and daily mean.

2.2. TRMM dataset

The present study used the TRMM 3B42 version 6 (chapter 3) and 7 (chapter 4) (Huffman et al. 2007) precipitation dataset to investigate spatial distribution of precipitation over the MC. This dataset is created by blending passive microwave data collected by the TRMM Microwave Imager (TMI), Special Sensor Microwave Imager (SSM/I), Advanced Microwave Scanning Radiometer for the Earth Observing System (AMSR-E), Advanced Microwave Sounding Unit B (AMSU-B), and IR data acquired by the international constellation of geosynchronous earth orbit (GEO) satellites, and based on calibration by the precipitation estimate of the TMI–PR combined algorithm. This product is created by merging the monthly accumulation with the monthly accumulated Climate Assessment and Monitoring System (CAMS) and Global Precipitation Climatology Centre (GPCC) rain gauge analysis. A description of the 3B42 algorithm is provided online (http://trmm.gsfc.nasa.gov/3b42.html). This dataset covers both temporally and spatially consecutive data in the domain 50°S to 50°N every 3 h, with horizontal resolution 0.25° × 0.25°.

The study also used the TRMM PR 2A25 version 7 data (Iguchi et al. 2000) for the period from 1998 to 2012 (15 years) to investigate spatial distribution of precipitation over the MC (Chapter 4). The study compiled the TRMM PR data into gridded data with a resolution of 0.15° × 0.15°. The study used the near-surface rain rate to examine the spatial distribution of precipitation over the MC. TRMM PR data with a 1.25° × 1.25° resolution, which is same resolution as the reanalysis data, were also used to calculate P for the atmospheric water budget.

2.3. Other datasets

To examine interactions between precipitation variability and atmospheric circulation, this study uses Japanese 25-year (1979–2004) reanalysis (JRA25)/Japan Meteorological Agency (JMA) Climate Data Assimilation system (JCDAS) on a 1.25° latitude–longitude grid (Onogi et al. 2007). With the exception of precipitation from the atmospheric water budget, all components were calculated using data from the JRA25/JCDAS. The high-spatial-resolution reanalysis data used here can provide detailed information on the atmospheric water cycle over the MC including complex land/ocean distributions that cannot be discerned in coarse reanalysis data. This study used the JRA25/JCDAS from 1998 to 2012 (15 years).

To investigate convective cloud variation associated with the MJO, Daily interpolated outgoing longwave radiation datasets from the National Oceanic and Atmospheric Administration (NOAA) Climate Prediction Center (CPC) (Liebmann and Smith 1996) from a 5-yr period (1999–2003) were also used. These datasets have spatial resolutions 2.5° × 2.5°.

In Chapter 4, the phase and amplitude of the MJO are defined according to the Real-time Multivariate MJO (RMM) index as described by Wheeler and Hendon (2004). This index is based on a pair of empirical orthogonal functions of the combined 850 hPa zonal wind, 200 hPa zonal wind, and satellite-observed OLR data averaged across the equator (15° S–15° N). The pair of principal component time series removed from the annual cycle and interannual variability components are called RMM1 and RMM2, respectively, and are used to define eight phases of MJO. Phases denote the period

when the center of convective activity (i.e., low-level convergence) is located near Africa (Phase 1); over the Indian Ocean (Phases 2 and 3); over the MC (Phases 4 and 5); over the western Pacific (Phases 6 and 7), and over the eastern Pacific (Phase 8).

2.4. Atmospheric water budget

Water budget calculations and data analyses were performed for the 15-year period from January 1998 to December 2012. The atmospheric water budget equation (Trenberth and Guillemot 1995) can be written as:

$$\langle\frac{\partial w}{\partial t}\rangle + \langle\nabla \cdot Q\rangle = \langle E - P\rangle, \quad (1)$$

where P is precipitation, E is evaporation and evapotranspiration, w is precipitable water content, and Q is the vertically integrated moisture flux vector, where its convergence (C) is given by $-\nabla \cdot Q$. The angled brackets denote the area average. Here, the precipitable water content (w) and vertically integrated moisture flux vector (Q) are given by:

$$w = \frac{1}{g}\int_{p_t}^{p_s} q dp \quad \text{and} \quad (2)$$

$$Q = \frac{1}{g}\int_{p_t}^{p_s} qV dp, \quad (3)$$

where q is the specific humidity, V is the horizontal wind vector, p_s is the pressure level at the surface, p_t is the pressure at the top of the atmosphere, and g is gravitational acceleration.

Vertical integration is performed from the ground (surface pressure level) to p_t (100 hPa). I also define the local water use ratio (LWR) from Equation (1) as follows:

$$\langle LWR \rangle = \langle \frac{1}{P}\left(P + \frac{\partial w}{\partial t} - C\right) \rangle \times 100\%. \quad (4)$$

The LWR indicates the contribution of the *E,* which is estimated as residual from the other components to the precipitation. The large LWR indicates that the fraction of precipitation in a region is sustained by local evaporation and evapotranspiration. On the other hand, the small LWR indicates that large-scale vapor convergence is dominant in the moisture feedback. The components of *C* and *w* are computed for every 6 h using the JRA25 dataset.

3. Modulation of the diurnal cycle of precipitation associated with the MJO observed by a dense hourly rain gauge network at Sarawak, Borneo

This chapter examines how the DCP is affected by MJO disturbances, along with its time–space characteristics over the ocean, coastal regions, and island interiors with particular reference to the major MC islands. Section 3.1 examines general features of DC characteristics using in situ data and TRMM data over the study region. Effects of the MJO on rainfall are based on daily rainfall data and are shown in Section 3.2. Impacts of the MJO on the DC based on rainfall amount, frequency, and intensity are described in Section 3.3. The DC of large-scale circulation associated with modulation of the DCP is presented in Section 3.4.

3.1. General features of precipitation activity over Borneo

Figure 3.1a shows the spatial distribution of 5-yr mean daily precipitation over the MC from TRMM. The overall spatial pattern shows heavier precipitation over land areas, e.g., Sumatra, New Guinea and Borneo, and less over surrounding oceans and open sea. The area of heaviest precipitation on Borneo appears in its western part (Sarawak). Figure 3.2a shows the spatial distribution of 5-yr mean daily precipitation amounts over Sarawak from the 50 precipitation stations. This areal contrast in precipitation differs from area to area (Fig. 3.1a). Precipitation data from TRMM

generally tend to be underestimated over land relative to that from *in situ* data (Nair et al. 2009; Yuan et al. 2012). These works also show that this tendency varies by area over the land, and the spatial pattern of precipitation is similar in both datasets. Precipitation amount from TRMM tends to overestimate (underestimate) in coastal (interior) areas relative to *in situ* data. The greatest precipitation appears in inland areas of the western mountains, and the least in the northern coastal area – at Miri (3) and Lambir Hills N. P. (4) (numbers refer to locations in Table 3.1 and Fig. 3.1b; precipitation in the two regions differs by a factor greater than two). Figure 3.2b shows spatial distributions of phase and amplitude of the 5-yr mean DCP from hourly precipitation data; maxima are indicated by the directions of arrows and amplitudes by their lengths. On the whole, an afternoon-to-night maximum (1600 to 2100 LT) is dominant in most regions. The peak time in southwest Sarawak (around 110 to 112°E) is during the evening (1600 to 1700 LT), and that of northeast Sarawak (around 114 to116°E) is at night (1900 to 2100 LT). Maximum precipitation is at midnight (0000 LT) in Bintulu (2), which is closest to the coast. In addition, Miri (3) and Lambir Hills N.P. (4), a few kilometers from the coastline in the northeast area, also experience precipitation near midnight (at 2300 and 0000 LT, respectively). Sungai Arau (16), about 30 km from the nearest coast, and Belaga (11), in central Sarawak, have precipitation peaks at 0100 and 0000 LT, respectively. The precipitation amount and time of occurrence of maximum diurnal precipitation exhibit large regional differences over Sarawak.

To classify the DCP pattern more objectively, Ward's cluster analysis was applied to 5-yr mean hourly precipitation. The minimum distance between clusters shows large difference of the distance between number 6 and 7 of clusters (Fig. 3.3). Therefore, the spatial pattern of precipitation in the region can be divided into seven categories (Table 3.1): The southwest category with one station (C-1); coastline category (C-2) with one station; northeast coastal area with two stations (C-3); interior plain to mountain categories (C-4, C-5, and C-6) with three, five and three stations respectively, and central plain category in the south (C-7) with five stations (Fig. 3.4). These seven precipitation classifications based on the mean DC pattern are similar to the categorized spatial pattern of precipitation using climatological pentad means for this region (Gomyo and Kuraji 2006). This suggests that seasonal and annual precipitation patterns depend on the regional DC pattern. Figure 3.4 shows the DC of 5-yr mean precipitation for the seven categories, which are averaged for the stations in each category. The DCs in all categories show a time of minimum precipitation during 0900–1100 LT, indicating that precipitation is suppressed in the morning over the entire region. The afternoon-to-nighttime precipitation peak propagates from coastal to interior areas in the following order from 1300 to 2100 LT: C-3, C-1, C-4, C-7, C-6 and C-5 (Fig. 3.2b). In the coastline and coastal categories, the midnight-to-morning precipitation peak is apparent at C-2 and C-3, occurring at 2300 and 0000 LT, respectively. The DC at C-3, which is a few kilometers from the coastline, shows features of both coastal (midnight to morning peak) and interior (afternoon to nighttime peak) areas. Additionally, the inland categories (C-4 to C-7) show different times of DC

peak and amplitude from region to region, though all peak times are in the late afternoon to nighttime. Although detailed characteristics of the DC patterns vary greatly by region, presumably because of complex terrain, characteristics of the DCP (time of maximum precipitation and its amplitude) can be grouped into two types – coastal (C-1 to C-3) and interior regions (C-4 to C-7).

The time of maximum precipitation strongly depends on distance from the coast. Scatter diagrams show the dependence of time of maximum precipitation in the 5-year dataset on distance from the coastline (Fig. 3.5). The regression line and correlation coefficient refer only to the afternoon-to-nighttime (1200–2200 LT) precipitation peaks, which are shown as crosses. The relationship between distance from the coast and time of maximum afternoon-to-nighttime precipitation shows significant ($P<0.05$) correlation ($r = 0.74$). Only a few stations, within about 30 km of the coastline, have double precipitation peaks, i.e., a large afternoon maximum and small midnight-to-morning maximum. This indicates that these near-coast areas receive precipitation from both afternoon-to-nighttime and midnight-to-morning systems.

3.2. Effects of the MJO on daily precipitation variation

Daily variation of the DCP over Sarawak is thought to be associated with variation in the large-scale circulation field. The seasonal cycle of precipitation over Borneo is weak compared with other tropical areas, as revealed by relatively low spatial resolution OLR data (Matsumoto 1997; Kumagai et al. 2005). However, Gomyo and Kuraji (2006) found a distinct climatological seasonal cycle of precipitation in southern

Sarawak (approximately corresponding to C-1 and C-7), using rain gauge data. They suggested that this seasonal cycle is caused by topographic effects. Figure 3.6 shows a time series of average daily precipitation at the 50 stations from 1999 to 2003. There is a weak seasonal cycle, with relatively heavy precipitation in the boreal winter. The northeasterly monsoon flow enhances precipitation and convective activity particularly over the South China Sea (Chang et al. 2005a; Chang et al. 2005g). The coastal region of the southern Sarawak (C-1 and C-7) is strongly affected by this seasonal cycle. The precipitation time series of these stations show distinct intraseasonal variations in addition to the seasonal cycle, which is dominant commonly over the entire Sarawak region. Spectral analysis using the fast Fourier transform (FFT) method was applied to the 5-day running mean daily precipitation from the entire 5-yr (1826 day) period. Figure 3.6 shows the power spectrum for this time series, revealing a dominant peak around 50 days and a secondary peak from 25–30 days. These correspond to the dominant periods of intraseasonal variations of large-scale convection in the MC (Hsu and Lee 2005; Zhang 2005). Figure 3.7 shows the spatial distribution of correlation between the 25-70 days 50 stations mean precipitation and the 25-70 days precipitation at each station. The 25-70 days variation of precipitation is pronounced over Sarawak. Over southwestern part of Sarawak, this timescale variation is relatively small compared with the other region. In contrast, the precipitation variability over interior region depends on the 25-70 days precipitation variation.

Temporal variation in circulation and large-scale convection associated with predominant intraseasonal variations of 50-day period in Borneo was examined by a

time-composite technique for the entire 5-year dataset. OLR data were adopted as a measure of deep convection associated with these MJO-related variations (Chang et al. 2005a). Twenty-six cycles with maximum and minimum events exceeding a standard deviation of 1.0 were selected for the composites, based on 25–70 day band-pass filtered anomalies of area-averaged OLR time series (110–117°E, 0–6°N; rectangular box in Fig. 3.1a). The 25–70 day OLR 5-yr time series shows significant ($P<0.05$) negative correlation with the 25–70 day daily mean precipitation 5-yr time series over the Sarawak region ($r = -0.50$). Fourteen cycles were selected for the composite in boreal summer (April-September), and 12 cycles for boreal winter (October-March). Eight phases make up each cycle. To retain sufficient sample sizes for both phases, active and break phases of MJO scale are defined by the period from phase 1 to 3 and that from phase 5 to 7, respectively.

Using the gauge datasets, the spatial distributions of daily precipitation in active and break phases over Sarawak are shown in Fig. 3.8a and 3.8b. In the active phase, Sarawak precipitation increases relative to the break phase, although the spatial pattern of large precipitation amounts in the interior mountains and southwest coastal areas does not change greatly in either phase. The largest difference is in the coastal region and foothills of the interior. Precipitation enhancement is particularly extreme near the coast. The spatial distribution of precipitation rate of change from active to break phase shows a clear difference (Fig. 3.8c). Coastal areas facing northwest show the largest precipitation change from the MJO break to active phase, whereas those facing north show less change. The interior mountain region of the island, with high precipitation,

shows even smaller changes. Thus, daily precipitation from gauges increases in the active phase region-wide, but more remarkably in the coastal areas, suggesting a stronger response to the MJO. Like Fig. 3.8a–c, Figure 3.8d–e shows a spatial distribution of daily precipitation, but the data are derived from the TRMM and cover all of Borneo and surrounding oceans. Overall, in both phases, TRMM overestimated (underestimated) precipitation in coastal (interior) regions, relative to the gauge data. This tendency is likely to hold even for the 5-yr mean DCP (Figs. 3.1 and 3.2a). The TRMM shows that precipitation over land and surrounding ocean increases in the active phase. In the surrounding ocean during this phase, the distribution of heavy precipitation area is extensive, from the coastline to open ocean. However, this distribution is limited to near-coastal areas in the break phase. Figure 3.8f shows the rate of change of TRMM precipitation from break to active phases. This rate is much greater over the ocean than over land. It was found that TRMM precipitation over land underestimates the impact of the MJO on precipitation, compared with that suggested by the gauge data. However, the common indication from both datasets is that the influence of the large-scale MJO on precipitation varies across oceanic, coastal land, and interior land areas.

3.3. Change of precipitation diurnal cycle associated with the MJO

Figure 3.9 shows modulation of the DCP attributed to the global-scale MJO for the seven categories (defined in Fig. 3.4). All categories show precipitation minima

around 1000 LT, as well as the DC in both active and break phases. They also show that hourly precipitation increases between break and active phases (except for minimum precipitation time). In the break phase, the precipitation peak from afternoon to nighttime is between 1200 and 1600 LT in the coastal categories (C-1 to C-3). This precipitation maximum propagates inland, e.g., categories C-4 to C-7 show the maximum between 1700 and 2000 LT. The precipitation peak from midnight to morning occurs at 0200 LT in categories 2 (C-2) and 3 (C-3). The second precipitation peak appears at 1400 LT in category 2 (C-2), although it is smaller than the other precipitation peaks. Category 1 (C-1) has a second maximum at 0800 LT, though this is not shown in the mean DC. In the active phase, the precipitation peak from afternoon to nighttime in the coastal categories remains unchanged. The DC in the interior categories (C-4 to C-7) indicates a remarkable precipitation increase from the break to active phase. The midnight to morning precipitation maxima is at 0000 LT in coastal categories (C-1 to C-3). Category 2 (C-2) has a small secondary precipitation maximum at 1200 LT, though a clear difference is not evident between active and break phases. This precipitation peak appears two hours earlier during the break phase, although the difference is small. In category 1 (C-1), the precipitation peak at 0000 LT in the active phase appears as a secondary precipitation maximum.

In the coastal region (C-1 to C-3), though the afternoon-to-nighttime precipitation maximum is not influenced by the MJO, that from midnight to morning is clearly so influenced. The midnight-to-morning precipitation peak in category 2 (C-2) doubles from the break to active phase. The precipitation minimum at 1800 LT (C-2 and

C-3), a boundary between the afternoon and midnight-to-morning precipitation systems, is only distinct during the break phase. In interior mountain regions (C-4, C-6 and C-7), the DC phase does not change between active and break phases, whereas its amplitude (precipitation amount) increases (decreases) in the active (break) phase. In addition, the DC in category 5 (C-5) seems to reflect some DC phase change. It is well known that the DC has a midnight-to-morning precipitation peak over the tropical ocean (Yang and Slingo 2001; Kikuchi and Wang 2008). The midnight-to-morning peak near the coast may be related to this oceanic peak. In fact, the MJO has more impact on precipitation over the ocean than over land (Fig. 3.8). As a result, the DC in coastal categories is modulated more strongly by the midnight-to-morning peak over the ocean than peaks in the island interior (C-4 to C-7). The difference of 5-yr mean precipitation shown in Fig. 3.4 (gray solid line in Fig. 3.9) from both phases shows that the DC in coastal regions depends more on the MJO than in the interior. Thus, change of the DCP in terms of amounts and phases from the MJO break to active phase exhibits different characteristics between coastal region and interior.

Figure 3.10 shows the DC of frequency and intensity of the precipitation composite for the seven categories. Precipitation frequency is defined by the number of precipitation days for each hour per total number of days (a percentage), and precipitation intensity is defined by precipitation amount per precipitation event for each hour in both phases, for each station. In all categories, precipitation frequency increases through the day from break to active phases. This tendency is remarkable. Over all interior categories (C-4 to C-7), the DC of intensity does not change between

phases. Hence, DC variation in both phases is represented by a change in frequency of precipitation between active and break phases. In the coastal categories (C-1 to C-3), however, the DCP intensity is clearly different between phases. In the break phase, this DC has large amplitude relative to the active phase. The afternoon-to-nighttime maximum of intensity in the break phase in coastal categories (C-1 to C-3) is stronger than in the active phase. In category 2 (C-2), the afternoon-to-nighttime peak time of intensity in the break phase is two hours earlier than in the active phase. This tendency is consistent with precipitation amount, as shown in Fig. 3.9.

Therefore, the change of DC between break and active phases in the interior region is explained by change in the DC of frequency. On the other hand, change of the DC in the coastal region is affected by both changes of frequency and of precipitation intensity. The DC in the coastal region is strongly affected by characteristics of the oceanic DC, where the impact of the large-scale cloud systems associated with the MJO is important.

3.4. Diurnal cycle of large-scale circulation associated with the MJO

This section is devoted to discussion on how the DC across the ocean, coastal zone and interior of Borneo Island is modulated by the MJO. Figure 3.11 shows a composite map of OLR and vertically integrated moisture flux anomalies for active and break phases. In the active phase, a low OLR anomaly appears over the entire MC, including the South China Sea, Borneo and particularly the ocean surrounding Borneo.

The South China Sea is dominated by a northeasterly moisture flux anomaly in this phase, which depends on the low-level wind. This moisture flux is presumably affected by island topography, and changes from northeasterly to northwesterly over the equatorial South China Sea between Sumatra and Borneo. As a result, the moisture flux anomaly seems to form a cyclonic circulation, centered over the southwest coast of Borneo. On the other hand, during the MJO break phase in this region, OLR and moisture flux anomalies show suppressed convection and an anticyclonic circulation, almost opposite to that of the active phase. It seems that anomalous deep convection systems during the active phase dominate the surrounding oceans more than Borneo.

Throughout one cycle (phases 1 to 8, not shown), negative OLR values (corresponding to cloud systems) propagate eastward, which are coupled with a baroclinic atmospheric structure with strong upper divergence. Simultaneously, low-level wind field anomalies change from westerly to easterly. With maximum precipitation over Borneo, low-level wind field anomalies transition from northeasterly to southwesterly, corresponding to enhanced cyclonic circulation anomalies associated with strengthened large-scale convection over Borneo and surroundings. Thus, precipitation variation in Borneo is modulated by large-scale convective variability, principally related to the MJO. Precipitation during the active phase in the coastal region (which is perpendicular to the westerlies) is strongly influenced by a low-level cyclonic anomaly, associated with the MJO (Fig. 3.11a).

The DCP is mainly controlled by the land-sea breeze, which is in turn controlled by differential thermal heating (Nitta and Sekine 1994; Chen and Takahashi 1995; Yang

and Slingo 2001). To examine moisture balance and thermodynamic characteristics of the island-scale convective system associated with the two MJO phases, composites of the DC for vertically integrated moisture flux divergence and atmospheric instability are produced in Fig. 3.12. The latter variable is defined as the difference of equivalent potential temperature between 850 hPa and 500 hPa. Figure 3.12a–d shows spatial patterns of average fields over Borneo and surrounding oceans at several times of the day (0800, 1400, 2000 and 0200 LT), as represented by means of the active and break phases. It was found that the DCs of these two atmospheric fields are clearly associated with the DCP. Because of strong surface heating by solar radiation and moisture increase in the lower troposphere over land, atmospheric instability is enhanced in the afternoon to evening (1400 to 2000 LT). Moisture flux divergence dominated by the low-level wind field is related to the land-sea breeze, more prominently on the west coast and interior of Borneo. Moisture flux convergence is enhanced over land at 2000 LT and surrounding ocean at 0200 LT. Differences of these fields from active to break phases are shown in Fig. 3.12e–h. The DC of these two fields show similar features in both phases, but DC amplitudes modulated by the large-scale atmospheric circulation vary between break and active phases, resulting in more active convection and heavier precipitation over the MC. Moisture flux convergence over the west coast of Borneo is more enhanced from midnight to morning (0200 to 0800 LT) in the active phase. This seems consistent with the strengthening of convergence between the offshore wind and low-level westerly anomaly related to the active MJO phase (Fig. 3.11). Furthermore, moisture flux convergence is enhanced throughout the day in the active phase. Water

vapor is transported from the ocean further into the interior. This contributes to the frequency increase in the interior from the break to active phase (Fig. 3.10). In the active phase, as a result of enhanced convective activity, atmospheric instability is suppressed over land through the day. This also suggests that the precipitation increase is attributable to the frequency increase rather than the intensity increase over land.

4. Effects of atmospheric water cycles over different time scales on the water balance over the Maritime Continent

This chapter estimates the land and ocean atmospheric water budget over the MC. To gain a better understanding of the processes responsible for heavy precipitation in the hydrological cycle, water budget analyses must be conducted separately for complex land and ocean areas in the MC. Section 4.1 shows the general features of the precipitation and moisture flux circulation fields between boreal summer and winter over the MC. Section 4.2 examines the climatological mean of the seasonal migration of the hydrological cycle over the MC. Effects on the hydrological cycle associated with the passage of MJO are shown in Section 4.3. The diurnal variability of the hydrological cycle represented as the variance of each component of the water budget is shown in Sections 4.4 and 4.5.

4.1. Seasonal changes in precipitation and moisture flux convergence

Figure 4.1 shows the climatological mean (1998–2012) of precipitation and atmospheric circulation fields for the boreal summer (May–September: MJJAS) and winter (November–March: NDJFM) over the MC. High precipitation values are observed over the Indian Ocean, Indian subcontinent, Bay of Bengal, Indochina Peninsula, and South China Sea, which is related to the southwesterly wind at 850 hPa

in MJJAS (Fig. 4.1a). On the other hand, precipitation is enhanced over Sumatra, Borneo, and New Guinea in NDJFM (Fig. 4.1c). Moisture flux convergence corresponds to precipitation activity in both seasons (Fig. 4.1b and 4.1d). High precipitation values are observed throughout the year in the MC, and precipitation centers tend to form over land rather than over oceans. In the boreal winter, precipitation is enhanced particularly over the west coast of Sumatra and the mountain regions in both Borneo and New Guinea.

Aside from Borneo, spatial patterns in moisture flux convergence over the MC correspond well with those of precipitation in both seasons. Note that moisture flux convergence over the Borneo region (including Borneo and its surrounding oceans) shows very weak convergence despite heavy precipitation throughout the year. This discrepancy between the spatial distribution of precipitation and moisture flux convergence over Borneo implies that the impact of large-scale circulation changes, such as the seasonal cycle, on precipitation is relatively small over Borneo compared with other MC regions.

To investigate the contribution of the diurnal precipitation cycle to total precipitation over the MC, the percentage of total variance explained by the DC is calculated from the TRMM 3B42 in Fig 4.2. A high percentage of the variance explained by the DC (>64%) extends from islands to surrounding oceans in both seasons. This index shows a weak seasonal change between land and coastal regions. The annual mean of the percentage of total variance explained by the DC is ~74% over major MC islands and >64% over the surrounding oceans within ~400 km of the coast.

The percentage of total variance is relatively small (<64%) over the ocean more than 400 km from land in the MC. The percentage of the total variance explained by the DC of moisture flux convergence is also higher over land and surrounding oceans. Therefore, the spatial characteristics of the atmospheric water cycle in the MC can be distinguished based on the distribution of the percentage of total variance explained by the DC.

The annual mean of the percentage of total variance explained by the diurnal precipitation cycle is calculated to classify the atmospheric water cycle more objectively. The threshold value of this percentage is defined as 66%. Figure 4.3 shows the domains for the atmospheric water budget analysis based on percentage variance in the diurnal precipitation cycle over the MC. These domains are defined as the Borneo region (BO), New Guinea region (NG), and the MC ocean region (MCO) (Fig. 4.3). BO and NG are further divided into land (BOL and NGL) and coastal regions (BOC and NGC).

4.2. Seasonal cycle of the regional atmospheric water budget

Figure 4.4 shows climatological monthly *P*, *C*, water vapor storage term, and the LWR for each domain. The temporal change in precipitable water content (PW) shows little variation and is negligible compared with other comportments. *P* and *C* show similar variations over all domains. There is a weak seasonal cycle, with relatively high *P* and *C* over BO during the boreal winter. As shown in Fig. 4.1, the northeasterly monsoon flow enhances precipitation and convective activity over BO. The seasonal cycles of *P* and *C* are clearly shown in the boreal winter over NG when large-scale

convection is enhanced by southward migration of the inter-tropical convergence zone (ITCZ). The contribution of *C* to *P* over land is smaller in BOL than in NGL throughout the year, and the contribution of *C* to *P* is higher over coastal areas (BOC and NGC) than over land (BOL and NGL). The difference between *P* and *C* is similar throughout the year in all domains. Thus, the seasonal LWR cycle shows a smaller variation than the *P* and *C* cycles.

The annual mean LWR over BOL exceeds 80%. In contrast, the annual mean LWR over NGL has a seasonal cycle associated with the cycles of *P* and *C*. The LWR differs from island to island (Table 4.1). In the NGL it increases in the boreal summer (to ~47%) and decreases in the boreal winter (to ~25%). *C* is stronger over coastal regions than over inland regions on both NG and BO, and thus the LWR is larger over islands than surrounding oceans. The annual mean LWR also differs between the MCO and coastal regions (BOC and NGC), and is ~38% in MCO, 50% in BOC, and 12% in NGC.

4.3. Impact of the MJO on the atmospheric water budget over the Maritime Continent

Deep convection and heavy precipitation on both NG and BO are enhanced in the boreal winter (Chang et al. 2005a; Zhou and Wang 2006; Ichikawa and Yasunari 2008). Precipitation/convection is also controlled by the MJO over the MC (Hsu and Lee 2005; Hidayat and Kizu 2010). Therefore, the active (break) phases of the MJO are

defined by the periods from Phases 3 to 5 (Phases 7–8 to 1) of the MJO index in the boreal winter.

Figure 4.5 shows precipitation, anomalies of 850 hPa wind vectors, vertically integrated moisture flux vectors, and convergence in the active and break periods in the boreal winter (NDJFM). During the active period, precipitation is enhanced over the ocean in the MC. In the break period, precipitation tends to decrease over the ocean. The difference in precipitation between the two periods is larger over the ocean and coastal regions compared with over land. The moisture flux convergence increases (decreases) over ocean regions during the active (break) period of the MJO, but this impact are not clear over BO. Therefore, the variations in moisture flux convergence from the active to the break phases show little intraseasonal difference over BO. The intraseasonal difference in moisture flux convergence is larger in NG than in BO, and the MJO has a stronger effect on precipitation and moisture flux convergence in the ocean regions than on island and coastal areas. Thus, the similar impact of MJO over the MC, which is not apparent over the BO, illustrates the effect associated with the seasonal change.

Figure 4.6 shows the time evolution of the water budget component anomalies, which are the difference from the NDJFM mean in each MJO phase over the five domains. Over all domains, P and C anomalies associated with the passage of MJO are enhanced for Phases 3 to 5 (active phases over the MC) and decrease from Phases 7 to 1 (break phases over the MC). The water vapor storage term is not affected by the MJO. The LWR anomalies are also small, which suggests that the MJO has little effect

compared with *P* and the *C*. For both BO and NG, *P* and *C* are larger over coastal regions (BOC and NGC) than over land (BOL and NGL) during active periods. *P* increases more over the MCO than over other domains, and is related to the rate of change from break to active periods.

Thus, the effect of the MJO on water budget components varies from region to region. *P* and *C* are less affected by the MJO over land than over both coastal regions and the MCO. The variation in *P* associated with the MJO coincides with the variation in *C* over all domains. On the other hand, the LWR is not clearly influenced at the MJO timescale in any of the domains. Therefore, MJO-induced changes in large-scale circulation can affect the fluctuations in *P* and *C,* which have a larger variation over coastal regions (BOC and NGC) and the MCO than over land (BOL and NGL). However, the contribution of local-scale effects (i.e., evaporation) on *P* is not clearly influenced by the MJO.

4.4. Effect of diurnal variations on the atmospheric water cycle over the Maritime Continent

Daily mean seasonal and MJO-cycle water budget variations are strongly related to *P* and *C* in all domains. The LWR also shows large differences between domains, and is highest over BOL compared with other domains. It is therefore likely that evaporation and evapotranspiration contribute to precipitation over BOL. On the other hand, the DC in precipitation is most pronounced over islands and coastal regions

compared with other timescales. It is therefore necessary to consider the water budget on a diurnal timescale over this region.

To further describe the DC of the water budget over the MC, Figure 4.7 shows anomalies from the daily NDJFM mean (at 0000 and 1200 UTC) for precipitation, the vertically integrated moisture flux vectors, and convergence. These times roughly correspond to morning and nighttime over the MC, respectively. Diurnal precipitation and moisture flux convergence cycles are clear over land (BOL and NGL) and coastal regions (BOC and NGC). The diurnal precipitation cycle is also pronounced, with late-afternoon to evening maxima over land, and nighttime to morning maxima over the surrounding seas. The moisture flux convergence cycle, dominated by the low-level wind field, is related to the land–sea breeze and is most prominent on islands and coastal regions. Moisture flux convergence is also enhanced over land in the afternoon to evening, and over the surrounding ocean in the nighttime to morning.

Over the MCO, there are no clear diurnal variations in precipitation and moisture flux convergence throughout the day. The water budget over BO and NG is dominated by a diurnal timescale, and is restricted to the island and its surroundings oceans. The daily mean timescale the moisture flux convergence is not clearly shown over the BO (Fig. 4.1). The region of weak moisture flux convergence corresponds to the region of pronounced moisture flux convergence at a diurnal timescale over BO. This overlap arises because moisture flux convergence and divergence cancel each other out throughout the course of the day. In contrast, the precipitation and moisture flux convergence at a diurnal and daily mean timescale are dominant over NG (Fig. 4.1).

The spatial distribution of diurnal precipitation and moisture flux convergence associated with the MJO has a similar pattern to the seasonal mean over the MC (figure not shown). Moisture flux convergence over BO, in particular, does not reflect the effect of the MJO (Fig. 4.5), but the DCs of precipitation and moisture flux convergence are clear and in-phase.

4.5. Effect of the diurnal atmospheric water cycle associated with the MJO

To clarify the influence of convective activity on daily mean variation and diurnal variation, Fig. 4.8 shows composite vertical–longitude diagrams of vertical velocity anomalies and their diurnal variance averaged between 5°S and 5°N (including BO in the active and break phases). In active phases, strengthened upward motion centered on 300 hPa associated with MJO convection propagates from the Indian Ocean to the MC. In break phases, the downward motion, also associated with MJO convection, moves westward from the MC to the Central Pacific. However, on a diurnal timescale the upward motion related to convective activity is distinct on islands and coastal regions in both phases over Borneo (120°E) and Sumatra (100°E). The notable velocity potential variability does not occur over the ocean in either active or break phases. The velocity potential variability is amplified and widespread over land and surroundings oceans in the active phase. The diurnal convection cycle associated with the land–sea breeze and localized mountain–valley circulation is clearly shown on land and coastal regions, and in island interiors during break phases. The relationship

between the MJO and the diurnal convection cycle is similar over NG and BO in both phases as shown in Fig. 4.9.

To examine the impact of the relationship between moisture transport on the MJO and diurnal timescales on the water budget over the MC, we split the vertically integrated moisture fluxes into stream function and velocity potential. The velocity potential component roughly approximates a moisture source and sink (Chen et al. 1995)s. Figure 4.10 shows a composite of the velocity potential and the diurnal variance of the vertically integrated moisture fluxes associated with the two MJO phases. The daily mean moisture fluxes converge or diverge corresponding to the active and break phases of the MJO over the MC. However, there is strong diurnal variance of the velocity potential around Sumatra, BO, and NG in both phases. Both timescales therefore have distinct influences on the water budget over the MC, and the effect of diurnal variations in moisture transport is especially important for the water budget of land and coastal regions.

5. Discussions

5.1. Modulation variations of the diurnal cycle of precipitation associated with the MJO between the interior and coastal regions

The spatial distributions of DCP were subdivided into seven categories based on the phase and amplitude of the DC using a 5-year mean precipitation. The coastal region (approximately 30 km from the coastline) has two precipitation maxima periods from afternoon to nighttime and midnight to morning. The interior region has only one maximum occurring during afternoon to nighttime. These precipitation maxima are likely generated by land–sea temperature differences and the resulting land–sea breeze convection systems (Houze et al. 1981; Nitta and Sekine 1994; Chen and Takahashi 1995; Yang and Slingo 2001). The variable characteristics of DCP between land and ocean over the MC were discussed by Kikuchi and Wang (2008). Here, the DCPs are further categorized into seven subdivisions of the coastal and interior regions based on *in situ* hourly precipitation data recorded over western Borneo.

I then investigated the impact of large-scale, eastward-moving MJO disturbances over a 25- to 70-day time scale on the DCP in this region. A seasonal cycle of low-level circulation fields, i.e., westerlies in boreal summer and northeasterlies in boreal winter, is dominant across the MC (Chang et al. 2005g). This seasonal cycle affects deep convection over the South China Sea and coastal Borneo associated with

the MJO throughout the year. The deep convection also appears to be associated with the MJO and other synoptic disturbances such as the Borneo vortex and cold surge in the boreal winter monsoon (Chang et al. 2005a). However, the time series of daily precipitation based on data from rain gauges over Sarawak shows a relatively weak seasonal cycle and distinct intraseasonal variations over the 25- to 70-day time scale throughout the year. A time–longitude section of OLR along the equator reveals that this intraseasonal variation of precipitation over Sarawak shown in Fig. 3.6 is associated with large-scale eastward-moving MJO disturbances. This indicates that the MJO disturbances have a strong effect on daily precipitation variation over this region throughout the year. The daily precipitation variation is also strongly controlled by the DC. Ichikawa and Yasunari (2006) showed that the DCP over Borneo is modulated by the change of low-level wind variations from westerly to easterly, dependent on the phase of the MJO. We also investigated how these MJO disturbances affect the DCP from coastal to interior regions of Sarawak based on the analysis of rain gauge data collected in this region.

The rain gauge data show larger precipitation amounts over land during the active phase of the MJO than the TRMM 3B42 data (see Fig. 3.8). This suggests that the TRMM data likely underestimate the effects of the MJO over land. Some previous studies reported the same tendency in precipitation underestimation between satellite and *in situ* data over land, but not in coastal regions (Nair et al. 2009; Yuan et al. 2012). Some recent studies also show that the TRMM PR data cannot adequately capture precipitation from shallow clouds in mountainous regions associated with local

mountain–valley circulations (Kwon et al. 2008; Kubota et al. 2009). The spatial pattern of gauge precipitation clearly shows the increase from the coastal to interior regions in the break to active MJO transition. However, the TRMM 3B42 data show that coastal precipitation changes are synchronized with those over the nearby ocean where the MJO disturbance effect is stronger than over the island interior. This tendency becomes more apparent in the boreal summer than in the boreal winter (not shown), because the other synoptic disturbances such as the Borneo vortex and cold surges are enhanced in the boreal winter (Chang et al. 2005a). However, the effect of MJO on the DCP appears frequently in both seasons. Thus, we can achieve a unified view of precipitation changes between the ocean, coastal areas, and interior of Borneo by combining the OLR data with data from TRMM 3B42 and the rain gauge network.

The rain gauge data clearly show that the DC strengthens during the MJO active phase and weakens during the break phase when there are no MJO disturbances. Phases of the DC are the same in both coastal and interior regions. An increase in precipitation is observed in all categories throughout the day during the active MJO phase, but the diurnal precipitation pattern does not change between phases. In earlier studies, the DC amplitude based on IR data was seen to decrease in the active phase over Borneo (Chen and Takahashi 1995) and the western Pacific warm pool (Sui and Lau 1992). This is possibly because of reduced thermal contrast between land and ocean and broad cloud coverage throughout the day during that period. However, the DCP based on rain gauge data clearly indicates enhanced precipitation during the MJO active phase. Comparable to our results, a study using the TRMM PR data also shows a weakened DC over land

on the MC revealing an underestimated effect of the MJO on the DC (Rauniyar and Walsh 2011). The DC has large regional variability over land. Using TRMM 3B42 and IR datasets, Tian et al. (2006) showed that the DC is enhanced in the active phase between ocean and land across the MC; however, the variation in MJO impacts between land and ocean that they found is small compared with our results. The maximum precipitation peak from IR data appears 2 or 3 h later in comparison to the *in situ* data, which is thought to be due to the presence of anvil clouds (Nitta and Sekine 1994; Chen and Takahashi 1995; Ohsawa et al. 2001). The maximum precipitation peak in the TRMM 3B42 data also appears later than data from Southeast China (Yuan et al. 2012) and that of TRMM PR in the tropics (Kikuchi and Wang 2008). Consequently, this bias between rain gauge and TRMM data, which may be caused by anvil clouds, may exist in our study region. In addition, the double peak of precipitation found near the coast in rain gauge data is not detected in any of the satellite data. MJO disturbances strongly influence the coastal precipitation stations and nearby ocean, meaning that only the midnight-to-morning precipitation peak at the coastal stations was strengthened. The frequency of precipitation events increases in all categories during active phases, whilst the intensity of each precipitation event changes during both phases, but only in the coastal and inland categories. The afternoon precipitation maximum over the coastal region hardly changes between phases, but the intensity of this short-lived precipitation peak is stronger during the break phase. The DC variations between coastal and interior regions associated with the MJO are also evidenced in atmospheric circulation and thermodynamic instability. The low-level westerly wind anomaly, which is related to

the active phase, transports more moisture to the interior region relative to the break phase. This increases atmospheric instability and the likelihood of precipitation events based on local topography. In particular, the midnight-to-morning precipitation maxima at coastal stations are strongly dependent on large-scale convective activity of the MJO.

5.2. Variations in the impacts of large-scale circulations on the atmospheric water cycle between Borneo and New Guinea

Hydrological cycles over the MC were subdivided into land, coastal, and ocean categories based on the diurnal variance in precipitation. In the two major island regions of Borneo (BO) and New Guinea (NG), the hydrological cycles over land in Borneo (BOL) and New Guinea (NGL), and coastal regions in Borneo (BOC) and New Guinea (NGC) are linked owing to the influence of the land–sea breeze. The seasonal change in moisture flux transport associated with large-scale circulation is small over BO compared with NG and the Maritime Continent Ocean (MCO). The seasonal cycle of the atmospheric water budget shows that precipitation is synchronized with moisture flux convergence over the entire study region. The cycle is relatively weak over BO and MCO compared with NG. Convergence, *C*, does not contribute to precipitation, *P*, over BOL regions throughout the year; however, LWR makes a contribution of approximately 85 % of the annual mean over BOL regions. Based on *in situ* observations, the LWR was found to range from 50 % (Kume et al. 2011) to 74% (Kumagai et al. 2005) in western BO. It is therefore surmised that the regional mean LWR over BOL is overestimated when compared with results from ground-based

values, which is consistent with the atmospheric water budget calculations. In NGL, however, the PPR is small because *P* depends on *C* in the wet season (NDJFM). The LWR also makes a relatively small contribution to the atmospheric water budget over the MC.

The diurnal variability in precipitation, moisture flux, and divergence is clearly pronounced over land and coastal regions on both major islands. The diurnal variation is generated by land–sea temperature contrasts and resulting land–sea breeze convection systems over the MC (Houze et al. 1981; Nitta and Sekine 1994; Kikuchi and Wang 2008; Biasutti et al. 2012). The moisture flux divergence (convergence) occurs between afternoon and morning (from midnight to morning) over coastal regions in BO and NG. It appears that the contributions of moisture flux convergence and divergence to precipitation, particularly over BO, balance out throughout the day. Over BO, the large-scale circulation has a weak influence on the seasonal water budget, but localized low-level circulation has a strong influence on the water cycle on diurnal timescales. Having said this, seasonal and diurnal processes dominate variability in the hydrological cycle over NG. The hydrological cycle in MCO depends solely on seasonal variations. Thus, it can be seen that the DC plays an important role in the exchange of water between island and coastal regions across the MC.

This study also investigated the impact of the MJO, a dominant mode of deep convection and heavy precipitation, on the water cycle of the MC. Precipitation and moisture flux convergence are modulated by the propagating MJO disturbance. This impact appears stronger in the MCO and is more pronounced in coastal areas (BOC and

NGC) when compared with land areas (BOL and NGL). During their passage over the MC, MJO convective cloud systems do not clearly change over land compared with over open seas (Hsu and Lee 2005; Wu and Hsu 2009). Additionally, the LWR does not show any variation associated with MJO.

The diurnal variation in the MC atmospheric water cycle associated with the MJO is characterized by enhanced moisture flux convergence from midnight to morning over coastal regions during the active MJO phase compared with break phases. The low-level wind anomaly in the active phase increases this convergence and produces heavy precipitation around midnight over coastal regions (Kanamori et al. 2013). The DC of convection and precipitation in both phases is clearly differentiated between land and coastal regions. Moisture flux convergence and divergence over BO and NG is also clear on diurnal timescales. Therefore, the effect of diurnal variation on moisture transportation is shown to be especially important in the hydrological cycle over these regions.

The effect of local-scale diurnal variations on the atmospheric water cycle is larger over BO than over NG. The atmospheric water cycle over NG depends on both large-scale variations, such as the MJO, and local-scale variations, such as the land–sea breeze. The modulation of diurnal precipitation by MJO disturbances is smaller over BOL (Kanamori et al. 2013) and larger over NGL (Ichikawa and Yasunari 2008). Over NG, the diurnal precipitation cycle is enhanced over the southwestern part of the island in the break phase of the MJO, whilst it is enhanced during the active phase of the MJO over the southwestern and northeastern part of island (Ichikawa and Yasunari 2008). It

is assumed that the shape (including topography) of the islands generates different water cycles in BO and NG.

6. Conclusions

This study shows that the MJO effect is relatively weak over the island interior owing to the strong DC here during both active and break phases. During their passage over the MC, MJO convective cloud systems did not clearly change over land when compared with open seas (Hsu and Lee 2005; Wu and Hsu 2009). In the winter monsoon season, Houze et al. (1981) reported that land breezes converge with low-level northeasterly monsoons to generate offshore convection. This develops into organized precipitation systems that drop heavy precipitation from midnight to morning over Northwest Borneo. The northeasterly wind tends to shift to westerly through dynamic interactions of monsoon flow and topography over this area of Borneo, possibly producing the convergence between low-level westerly and land breezes here. The low-level westerly anomaly in the active phase intensifies this convergence and causes heavy precipitation around midnight over the coastal region. At that time, the occurrence of downslope winds may also be controlled by a mountain–valley wind system as simulated for a case in Southwest Borneo, which can also be referred to as Kalimantan (Wu et al. 2008). Another possible mechanism may be the development of propagating storms along mountain slopes. This is triggered by the intrusion of cold air by gravity currents caused by interaction between the cold pool from the convection and ambient near-surface winds (Satomura 2000). In addition to the propagating systems associated with the mountain range, gravity waves caused by a strong diurnal signal over coastal land have been shown to be important for offshore propagation (Yang and

Slingo 2001; Mapes et al. 2003). The surface wind from land to coastal regions organized by these topographic processes may also interact with the land breeze around midnight. However, the enhanced afternoon precipitation peak associated with the increased precipitation frequency in the island interior suggests an enhanced upslope wind through a strengthened moist westerly wind during the MJO active phase. The effect of the MJO on the DC over and around Borneo is thereby clearly different between ocean, coastal, and interior regions. It has been proposed that the DC precipitation peak propagates from the coastal to offshore region (Houze et al. 1981; Yang and Slingo 2001; Mapes et al. 2003; Yang and Smith 2006), which is likely intensified by the westerly wind anomaly during the active phase. To summarize the overall features of convection and precipitation over the ocean, schematics of the coastal and interior regions of Borneo are provided in Fig. 3.13.

The impact of MJO large-scale disturbances on the DC appears stronger in the midnight-to-morning precipitation maximum over coastal regions. More localized cloud/rain systems are dominant in the island interior during both break and active MJO phases. The DCP frequency increases over land, as increased water vapor is transported from the nearby ocean thus increasing moist static instability. The DCP intensity is only enhanced in the coastal region during the active phase, modulated by large-scale cloud/rain systems of the MJO. This variable influence of the MJO between coast and island interior is very likely attributable to the differing effects of the land–sea breeze, mountainous topography, and tropical rainforest surface cover. How the enhanced DCP over Borneo associated with the MJO might change the MJO system itself could be

another important issue of future study.

The atmospheric water cycle in Borneo is restricted spatially to land and coastal areas. The effect of moisture transport from coastal areas is small because the daytime land–sea breeze counteracts the inland movement of moisture. This means that the LWR is therefore high over Borneo compared with other regions. Evapotranspiration from tropical rainforest surface cover plays a major role in the maintenance of high precipitation over Borneo and increases the LWR over Borneo land areas. Kumagai et al. (2005) suggested that most precipitation is recycled from terrestrial evapotranspiration in these areas. The effect of evapotranspiration on the hydrological cycle at this timescale could not be accurately estimated in this work because the local solar time over the MC does not correspond to the 6-h reanalysis data available.

Given that rainforests are a major driver of the hydrological cycle, it follows that changes in forest cover affect the atmospheric water balance (Bonan 2008; Aragao 2012). Modeling work has illustrated the effect of deforestation on local precipitation leading to both a decrease (Kanae et al. 2001; Yasunari et al. 2006) and an increase (Spracklen et al. 2012). It is, therefore, important that future research includes an estimate of the diurnal evapotranspiration cycle over Borneo. In addition, the DC of precipitation and convection in reanalysis data must be used with caution because convective parameterizations employed by global reanalysis data have a quick trigger that initiates weak convection in the afternoons over land despite the supply of moisture for the observed precipitation maxima (Ruane and Roads 2007). A numerical simulation by regional and cloud-resolving models would help to further understand these

processes.

Schematics of the atmospheric water cycles over Borneo (Fig. 4.11) and New Guinea (Fig. 4.12) are provided to summarize the overall features. The hydrological cycle shows that large-scale circulation variations, such as the seasonal cycle and the MJO, have a lesser effect over Borneo than over New Guinea. However, the impact of DC on regional scale circulation and water exchange between land and coastal regions is pronounced over both islands. This shows that the local water use ratio is higher over Borneo than over New Guinea, which may be related to a stronger diurnal variation in the atmospheric water cycle that results from higher evapotranspiration over tropical rainforests.

Acknowledgment

I would like to express my deepest gratitude to Prof. Tetsuzo Yasunari of Research Institute for Humanity and Nature for his invaluable suggestions and continuous encouragement throughout my research activities. Even after my graduation from Graduate school of Environmental Studies, Nagoya University, he continuously gave many advices and supports about my study. I could not have done it without him. I am also indebt to Prof. Matsumoto in Tokyo Metropolitan University whose meticulous comments and supports were an enormous help to me. I would like to express my gratitude to Prof. Tomo'omi Kumagai of Hydrospheric Atmospheric Research Center (HyARC), Nagoya University for numerous valuable comments and suggestions. His advices and encouragements were essential to finish this work. I would like to give heartfelt thanks to Dr. Hatsuki Fujinami in HyARC whose comments and suggestions were innumerably valuable throughout the course of my study. I am also gratitude to Prof. Tetsuya Hiyama and Prof. Hirohiko Masunaga in HyARC for many helpful discussions and comments. Special thanks are extended to Dr. Hiroki Ichikawa for inspiring discussions and comments. I would also like to express my gratitude to my parents and wife for their moral support and warm encouragements. Finally, I would like to express gratitude to my colleagues for their encouragement and support.

List of references

Aragao, L. E. O. C., 2012: The rainforest's water pump. *Nature*, **489,** 217-218.

Biasutti, M., S. E. Yuter, C. D. Burleyson, and A. H. Sobel, 2012: Very high resolution rainfall patterns measured by TRMM precipitation radar: seasonal and diurnal cycles. *Clim. Dynam.*, **39,** 239-258, doi: 10.1007/S00382-011-1146-6.

Bonan, G. B., 2008: Forests and climate change: Forcings, feedbacks, and the climate benefits of forests. *Science*, **320,** 1444-1449, doi: 10.1126/Science.1155121.

Chang, C. P., P. A. Harr, and H. J. Chen, 2005a: Synoptic disturbances over the equatorial South China Sea and western Maritime Continent during boreal winter. *Mon. Wea. Rev.*, **133,** 489-503.

Chang, C. P., Z. Wang, J. McBride, and C. H. Liu, 2005b: Annual cycle of Southeast Asia - Maritime continent rainfall and the asymmetric monsoon transition. *J. Climate*, **18,** 287-301.

Chen, T. C., and K. Takahashi, 1995: Diurnal variation of outgoing long-wave radiation in the vicinity of the South China Sea: Effect of intraseasonal oscillation. *Mon. Wea. Rev.*, **123,** 566-577.

Chen, T. C., J. M. Chen, and J. Pfaendtner, 1995: Low-frequency variations in the atmospheric branch of the global hydrological cycle. *J. Climate*, **8,** 92-107.

Goessling, H. F., and C. H. Reick, 2011: What do moisture recycling estimates tell us? Exploring the extreme case of non-evaporating continents. *Hydrol. Earth Syst. Sc.*, **15,** 3217-3235, doi: 10.5194/Hess-15-3217-2011.

Gomyo, M., and K. Kuraji, 2006: Spatial distribution of seasonal variation in rainfall in the state of Sarawak, Malaysia. *J. Japan Soc. Hydrol. Water Resour.*, **19,** 128-138.

Hamada, J. I., M. D. Yamanaka, S. Mori, Y. I. Tauhid, and T. Sribimawati, 2008: Differences of rainfall characteristics between coastal and interior areas of central western Sumatera, Indonesia. *J. Meteor. Soc. Japan*, **86,** 593-611.

Hamada, J. I., M. D. Yamanaka, J. Matsumoto, S. Fukao, P. A. Winarso, and T. Sribimawati, 2002: Spatial and temporal variations of the rainy season over Indonesia and their link to ENSO. *J. Meteor. Soc. Japan*, **80,** 285-310.

Hidayat, R., and S. Kizu, 2010: Influence of the Madden-Julian Oscillation on Indonesian rainfall variability in austral summer. *Int. J. Climatol.*, **30,** 1816-1825, doi: 10.1002/Joc.2005.

Houze, R. A., S. G. Geotis, F. D. Marks, and A. K. West, 1981: Winter monsoon convection in the vicinity of north Borneo. Part I: Structure and time variation of the clouds and precipitation. *Mon. Wea. Rev.*, **109,** 1595-1614.

Hsu, H. H., and M. Y. Lee, 2005: Topographic effects on the eastward propagation and initiation of the Madden-Julian oscillation. *J. Climate*, **18,** 795-809.

Huffman, G. J., and Coauthors, 2007: The TRMM multisatellite precipitation analysis (TMPA): Quasi-global, multiyear, combined-sensor precipitation estimates at fine scales. *J. Hydrometeor.*, **8,** 38-55, doi: 10.1175/Jhm560.1.

Ichikawa, H., and T. Yasunari, 2006: Time-space characteristics of diurnal rainfall over Borneo and surrounding oceans as observed by TRMM-PR. *J. Climate*, **19,** 1238-1260.

Ichikawa, H., and T. Yasunari, 2008: Intraseasonal variability in diurnal rainfall over New Guinea and the surrounding oceans during austral summer. *J. Climate*, **21,** 2852-2868, doi: 10.1175/2007jcli1784.1.

Iguchi, T., T. Kozu, R. Meneghini, J. Awaka, and K. Okamoto, 2000: Rain-profiling algorithm for the TRMM precipitation radar. *J. Appl. Meteor.*, **39,** 2038-2052.

Kanae, S., T. Oki, and K. Musiake, 2001: Impact of deforestation on regional precipitation over the Indochina Peninsula. *J. Hydrometeor.*, **2,** 51-70.

Kanamori, H., T. Yasunari, and K. Kuraji, 2013: Modulation of the diurnal cycle of rainfall associated with the MJO observed by a dense hourly rain gauge network at Sarawak, Borneo. *J. Climate*, **26,** 4858-4875, doi: 10.1175/Jcli-D-12-00158.1.

Kikuchi, K., and B. Wang, 2008: Diurnal precipitation regimes in the global tropics. *J. Climate.*, **21,** 2680-2696, doi: 10.1175/2007jcli2051.1.

Kubota, T., S. Shige, K. Aonashi, and K. Okamoto, 2009: Development of nonuniform beamfilling correction method in rainfall retrievals for passive microwave radiometers over ocean using TRMM observations. *J. Meteor. Soc. Japan*, **87,** 153-164, doi: 10.2151/Jmsj.87a.153.

Kumagai, T., H. Kanamori, and T. Yasunari, 2013: Deforestation-induced reduction in rainfall. *Hydrol Process*, **27,** 3811-3814, doi: 10.1002/Hyp.10060.

Kumagai, T., and Coauthors, 2005: Annual water balance and seasonality of evapotranspiration in a Bornean tropical rainforest. *Agr. For. Meteor.*, **128,** 81-92, doi: 10.1016/J.Agrformet.2004.08.006.

Kume, T., and Coauthors, 2011: Ten-year evapotranspiration estimates in a Bornean

tropical rainforest. *Agr. For. Meteor.*, **151,** 1183-1192, doi: 10.1016/J.Agrformet.2011.04.005.

Kwon, E. H., B. J. Sohn, D. E. Chang, M. H. Ahn, and S. Yang, 2008: Use of numerical forecasts for improving TMI rain retrievals over the mountainous area in Korea. *J Appl Meteorol Clim*, **47,** 1995-2007, doi: 10.1175/2007jamc1857.1.

Lin, J. L., B. Mapes, M. H. Zhang, and M. Newman, 2004: Stratiform precipitation, vertical heating profiles, and the Madden-Julian oscillation. *J. Atmos. Sci.*, **61,** 296-309.

Madden, R. A., and P. R. Julian, 1971: Detection of a 40-50 day oscillation in zonal wind in tropical Pacific. *J. Atmos. Sci.*, **28,** 702-708.

Madden, R. A., and P. R. Julian, 1972: Description of global-scale circulation cells in tropics with a 40-50 day period. *J. Atmos. Sci.*, **29,** 1109-1123.

Madden, R. A., and P. R. Julian, 1994: Observations of the 40-50-day tropical oscillation - A Review. *Mon. Wea. Rev.*, **122,** 814-837.

Mapes, B. E., T. T. Warner, and M. Xu, 2003: Diurnal patterns of rainfall in northwestern South America. Part III: Diurnal gravity waves and nocturnal convection offshore. *Mon. Wea. Rev.*, **131,** 830-844.

Matsumoto, J., 1997: Seasonal transition of summer rainy season over indochina and adjacent monsoon region. *Adv Atmos Sci*, **14,** 231-245.

Murakami, M., 1983: Analysis of the deep convective activity over the western Pacific and Southeast Asia. Part I: Diurnal variation. *J. Meteor. Soc. Japan*, **61,** 60-76.

Nair, S., G. Srinivasan, and R. Nemani, 2009: Evaluation of multi-satellite TRMM

derived rainfall estimates over a western state of India. *J. Meteor. Soc. Japan*, **87,** 927-939, doi: 10.2151/Jmsj.87.927.

Neale, R., and J. Slingo, 2003: The maritime continent and its role in the global climate: A GCM study. *J. Climate*, **16,** 834-848.

Nitta, T., and S. Sekine, 1994: Diurnal variation of convective activity over the tropical western Pacific. *J. Meteor. Soc. Japan*, **72,** 627-641.

Ohsawa, T., H. Ueda, T. Hayashi, A. Watanabe, and J. Matsumoto, 2001: Diurnal variations of connective activity and rainfall in tropical Asia. *J. Meteor. Soc. Japan*, **79,** 333-352.

Oki, T., and K. Musiake, 1994: Seasonal change of the diurnal cycle of precipitation over Japan and Malaysia. *J. Appl. Meteor.*, **33,** 1445-1463.

Onogi, K., and Coauthors, 2007: The JRA-25 reanalysis. *J. Meteor. Soc. Japan*, **85,** 369-432.

Peatman, S. C., A. J. Matthews, and D. P. Stevens, 2014: Propagation of the Madden-Julian Oscillation through the Maritime Continent and scale interaction with the diurnal cycle of precipitation. *Q. J. R. Meteorol. Soc.*, **140,** 814-825, doi: 10.1002/Qj.2161.

Ramage, C. S., 1968: Role of a tropical "maritime continent" in atmospheric circulation. *Mon. Wea. Rev.*, **96,** 365-370.

Rauniyar, S. P., and K. J. E. Walsh, 2011: Scale interaction of the diurnal cycle of rainfall over the Maritime Continent and Australia: Influence of the MJO. *J. Climate*, **24,** 325-348, doi: 10.1175/2010jcli3673.1.

Ruane, A. C., and J. O. Roads, 2007: The diurnal cycle of water and energy over the Continental United States from three reanalyses. *J. Meteor. Soc. Japan*, **85A,** 117-143, doi: 10.2151/Jmsj.85a.117.

Satomura, T., 2000: Diurnal variation of precipitation over the Indo-China Peninsula: Two-dimensional numerical simulation. *J. Meteor. Soc. Japan*, **78,** 461-475.

Spracklen, D. V., S. R. Arnold, and C. M. Taylor, 2012: Observations of increased tropical rainfall preceded by air passage over forests. *Nature*, **489,** 282-U127, doi: 10.1038/Nature11390.

Sui, C. H., and K. M. Lau, 1992: Multiscale phenomena in the tropical atmosphere over the western Pacific. *Mon. Wea. Rev.*, **120,** 407-430.

Sui, C. H., K. M. Lau, Y. N. Takayabu, and D. A. Short, 1997: Diurnal variations in tropical oceanic cumulus convection during TOGA COARE. *J. Atmos. Sci.*, **54,** 639-655.

Tian, B. J., D. E. Waliser, and E. J. Fetzer, 2006: Modulation of the diurnal cycle of tropical deep convective clouds by the MJO. *Geophys. Res. Lett.*, **33,** L20704, doi: 10.1029/2006GL027752.

Trenberth, K. E., and C. J. Guillemot, 1995: Evaluation of the global atmospheric moisture budget as seen from analyses. *J. Climate.*, **8,** 2255-2272.

Waliser, D. E., B. J. Tian, X. S. Xie, W. T. Liu, M. J. Schwartz, and E. J. Fetzer, 2009: How well can satellite data characterize the water cycle of the Madden-Julian Oscillation? *Geophys. Res. Lett.*, **36,** L21803, doi:10.1029/2009GL040005.

Wheeler, M. C., and H. H. Hendon, 2004: An all-season real-time multivariate MJO

index: Development of an index for monitoring and prediction. *Mon. Wea. Rev.*, **132,** 1917-1932.

Williams, M., and R. A. Houze, 1987: Satellite-Observed Characteristics of Winter Monsoon Cloud Clusters. *Mon. Wea. Rev.*, **115,** 505-519.

Wu, C. H., and H. H. Hsu, 2009: Topographic influence on the MJO in the Maritime Continent. *J. Climate*, **22,** 5433-5448, doi: 10.1175/2009jcli2825.1.

Wu, P. M., M. D. Yamanaka, and J. Matsumoto, 2008: The formation of nocturnal rainfall offshore from convection over western Kalimantan (Borneo) Island. *J. Meteor. Soc. Japan*, **86,** 187-203.

Yang, G. Y., and J. Slingo, 2001: The diurnal cycle in the tropics. *Mon. Wea. Rev.*, **129,** 784-801.

Yang, S., and E. A. Smith, 2006: Mechanisms for diurnal variability of global tropical rainfall observed from TRMM. *J. Climate.*, **19,** 5190-5226.

Yasunari, T., K. Saito, and K. Takata, 2006: Relative roles of large-scale orography and land surface processes in the global hydroclimate. Part I: Impacts on monsoon systems and the tropics. *J. Hydrometeor.*, **7,** 626-641.

Yuan, W. H., R. C. Yu, M. H. Zhang, W. Y. Lin, H. M. Chen, and J. Li, 2012: Regimes of diurnal variation of summer rainfall over subtropical East Asia. *J. Climate*, **25,** 3307-3320, doi: 10.1175/Jcli-D-11-00288.1.

Zhang, C. D., 2005: Madden-Julian oscillation. *Rev. Geophys.*, **43,** RG2003, doi: 10.1029/2004rg000158.

Zhou, L., and Y. Q. Wang, 2006: Tropical Rainfall Measuring Mission observation and

regional model study of precipitation diurnal cycle in the New Guinean region. *J Geophys Res.*, **111,** D17104, doi: 10.1029/2006jd007243.

Tables and Figures

Table 3.1. Locations and details for 20 hourly precipitation stations.

No.	Station Name	Lognitude (E)	Latitude (N)	Distance (Km)	Elevation (m)	Category
1	Kuching	110.33	1.48	20	22	C-1
2	Bintule	113.03	3.20	2	3	C-2
3	Miri	113.98	4.33	3	17	C-3
4	Lambir Hills N.P.	114.05	4.20	15	59	
5	Lama, Long	114.40	3.76	75	75	C-4
6	Seridan, Long	115.06	3.98	101	192	
7	Bareo	115.46	3.74	148	1005	
8	Lio Matu	115.22	3.17	186	285	C-5
9	Subing, Long	114.27	3.33	95	35	
10	Lidam, Long	114.65	2.34	201	515	
11	Belaga	113.78	2.71	98	40	
12	Merit, Nanga	113.09	2.27	96	30	
13	Moh, Long	115.07	3.05	181	250	C-6
14	Akah, Long	114.79	3.32	139	135	
15	Pilah, Long	114.43	3.49	95	56	
16	Sungai Arau	112.57	2.31	76	82	C-7
17	Sibu	111.97	2.25	70	8	
18	Sri Aman	111.45	1.22	65	10	
19	Pantu	111.11	1.14	45	21	
20	Bunan Gega	110.54	0.92	77	70	

Table 4.1. Climatological (1998–2012) mean of the local water use ratio (LWR) (%) in the boreal summer (MJJAS: May–September), boreal winter (NDJFM: November-March), and annual mean over each region.

Region	MJJAS	NDJFM	Annual
Borneo land (BOL)	96.64	80.54	84.67
Borneo coast (BOC)	72.89	36.04	49.53
New Guinea land (NGL)	46.98	24.51	32.84
New Guinea coast (NGC)	18.53	5.19	11.96
Maritime continent ocean (MCO)	47.29	28.60	37.95

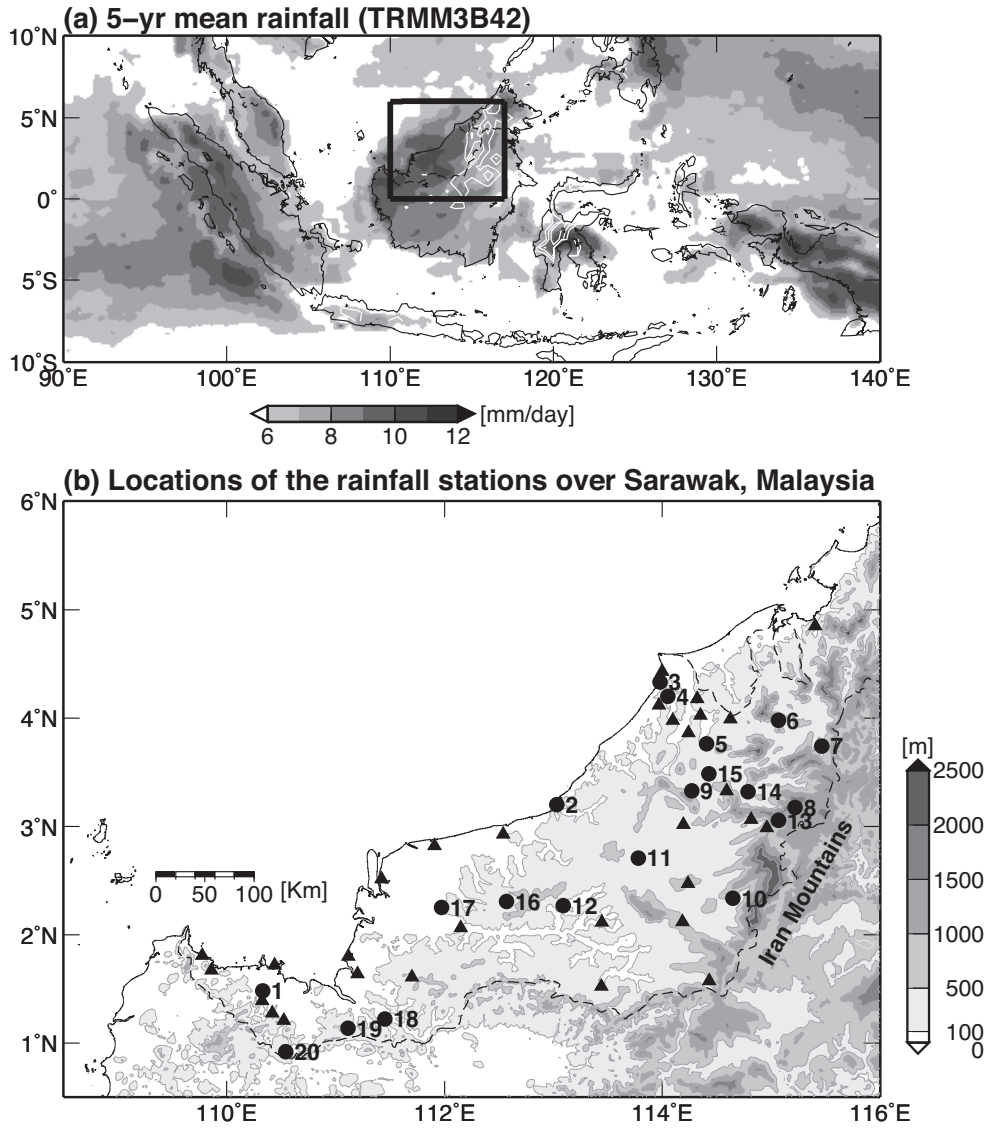

Figure 3.1. (a) Distribution of 5-yr mean daily precipitation amounts over Maritime Continent using TRMM 3B42 datasets from 1999 to 2003. Orography is shown by white contour with interval 500 m, beginning at 500 m. (b) Locations of 30 daily precipitation stations (black triangles) and 20 hourly precipitation stations (black circles) in Sarawak, Malaysia. Numbers correspond to hourly rain gauges described in Table 3.1. Rectangular box is area within which area-mean OLR time series were calculated.

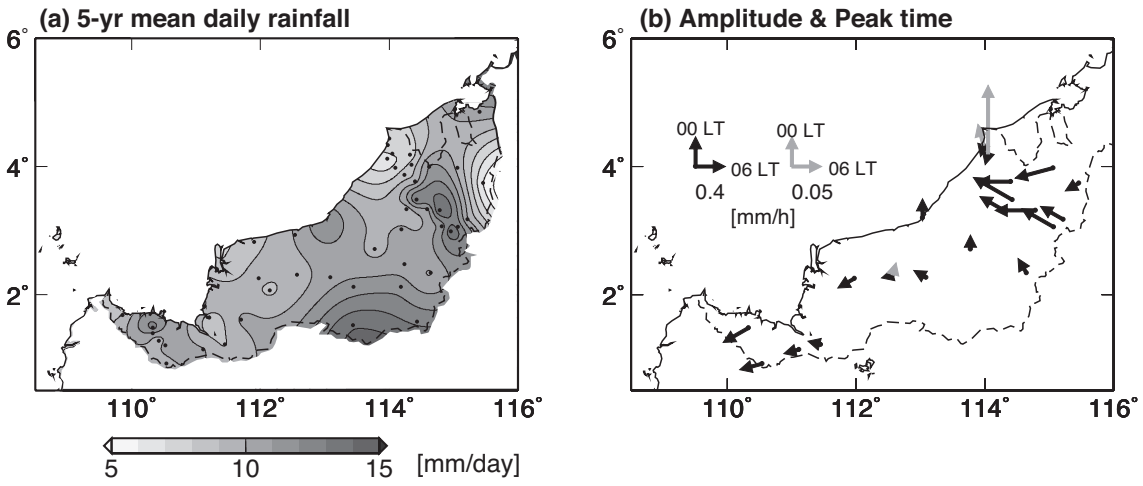

Figure 3.2. (a) Distribution of 5-yr mean daily precipitation amount (mm/day) over Sarawak, using 50 precipitation stations from 1999 to 2003. (b) Time of maximum precipitation of 20 hourly precipitation stations, for 5-yr mean. Vector orientation indicates local time of maximum precipitation, and length indicates deviation from daily mean (mm/h). Black and gray vectors represent primary and secondary maxima, respectively, which are defined from daily mean precipitation.

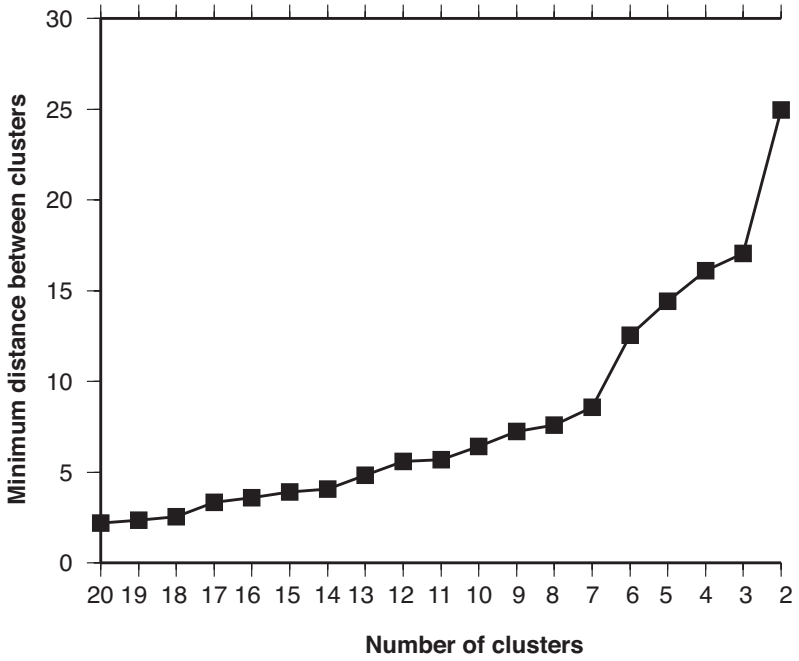

Figure 3.3. Sequence of similarities in which clusters merged for the average linkage between the clusters method.

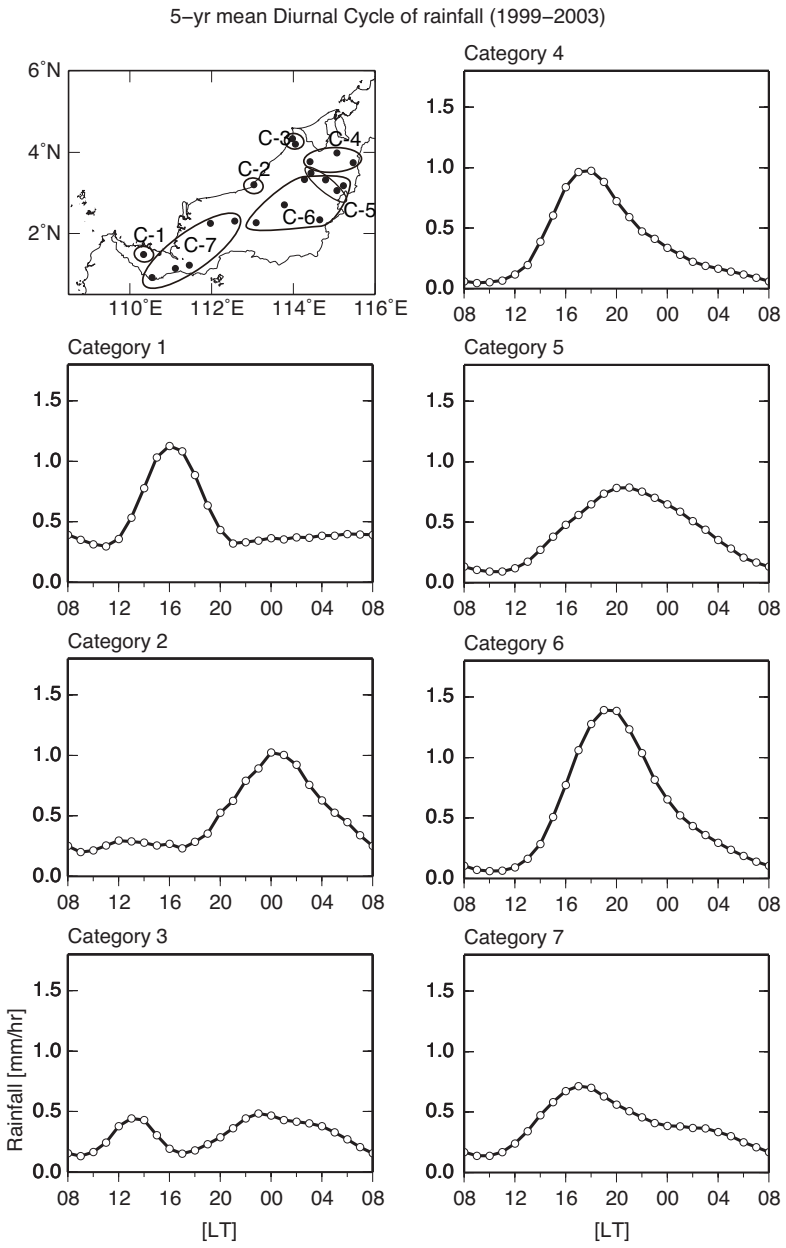

Figure 3.4. 5-yr mean DCP in seven categories. Numbers correspond to rain stations described in Table 3.1. Thick black solid lines indicate average precipitation of all stations in each category. Top left panel shows distribution of the seven categories over Sarawak.

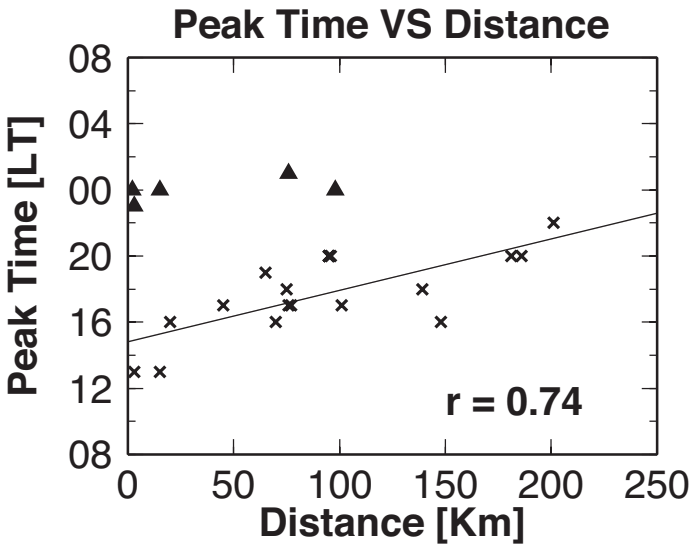

Figure 3.5. Scatter diagram of peak time of precipitation versus distance from the coast, for 5-yr mean DC of the 20 hourly stations. Crosses and triangles indicate afternoon–to-nighttime and midnight- to-morning precipitation peaks, respectively. Regression line and correlation coefficient indicate correlation between afternoon-to-nighttime peaks and distance from the coast.

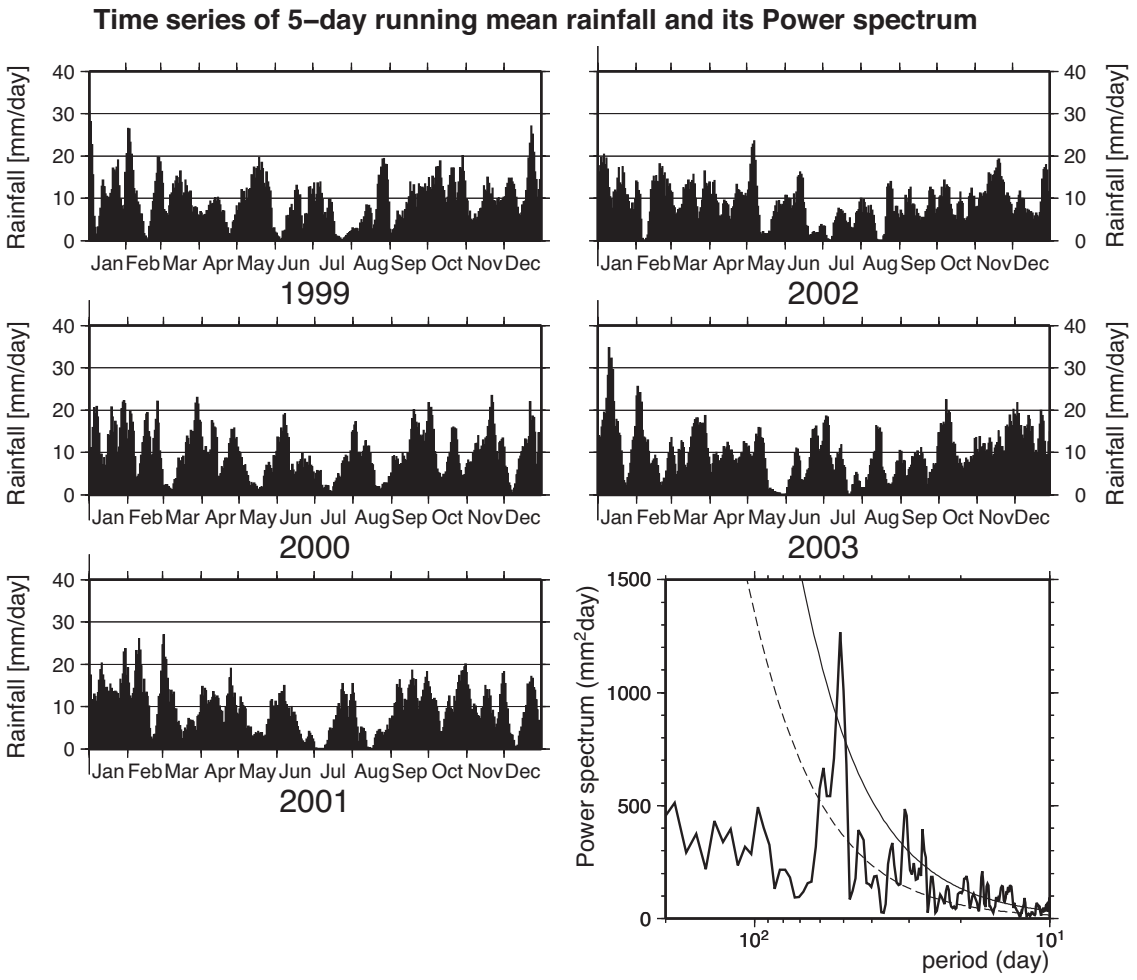

Figure 3.6. Time series of 5-day running mean precipitation (mm/day), averaged over 1999–2003 from rain gauge observations at 50 stations. Bottom right panel shows power spectrum of 5-day running mean precipitation averaged at 50 precipitation stations. Dashed line indicates red-noise spectrum, and solid line shows 95% significance level.

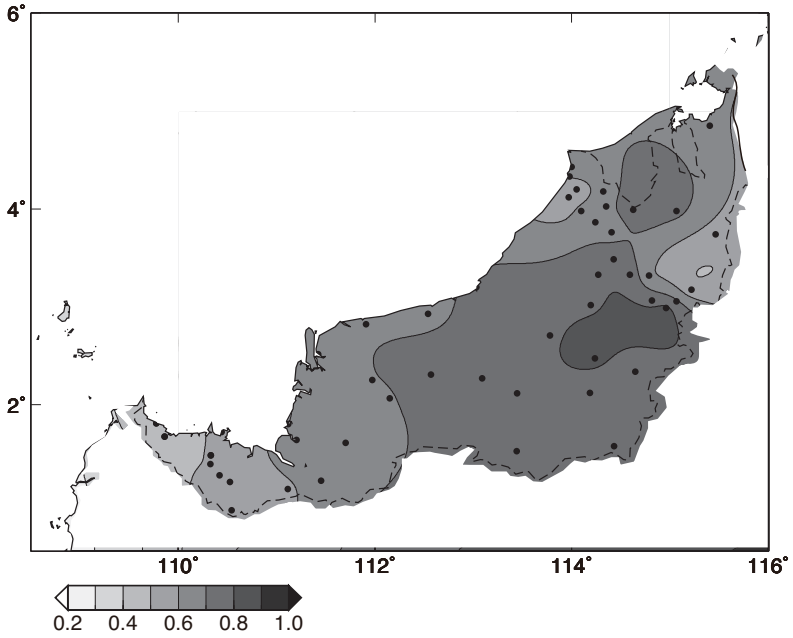

Figure 3.7. The spatial distribution of the correlation between the 25-70 days 50 stations mean precipitation and the 25-70 days precipitation at each station from 1999 to 2003. Over all stations indicate over significant at the 98% confidence level.

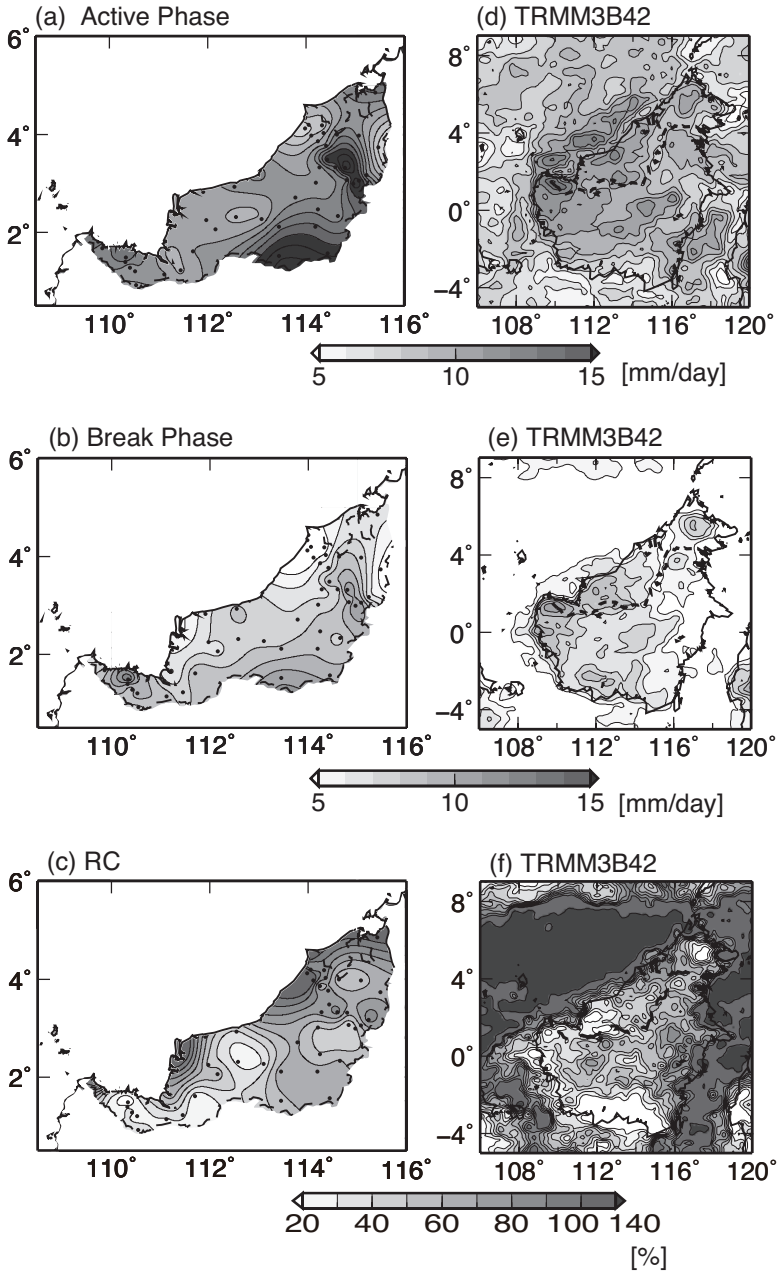

Figure 3.8. Composites of daily precipitation in (a) active phase, and (b) break phase over Sarawak, based on 50 precipitation stations. (c) Spatial distribution of rate of change (%) in precipitation from active to break phase, which is defined as [(active phase)/(break phase) −1] × 100. (d) to (f) Same as (a) to (c), but based on TRMM 3B42 data over Borneo and surrounding ocean.

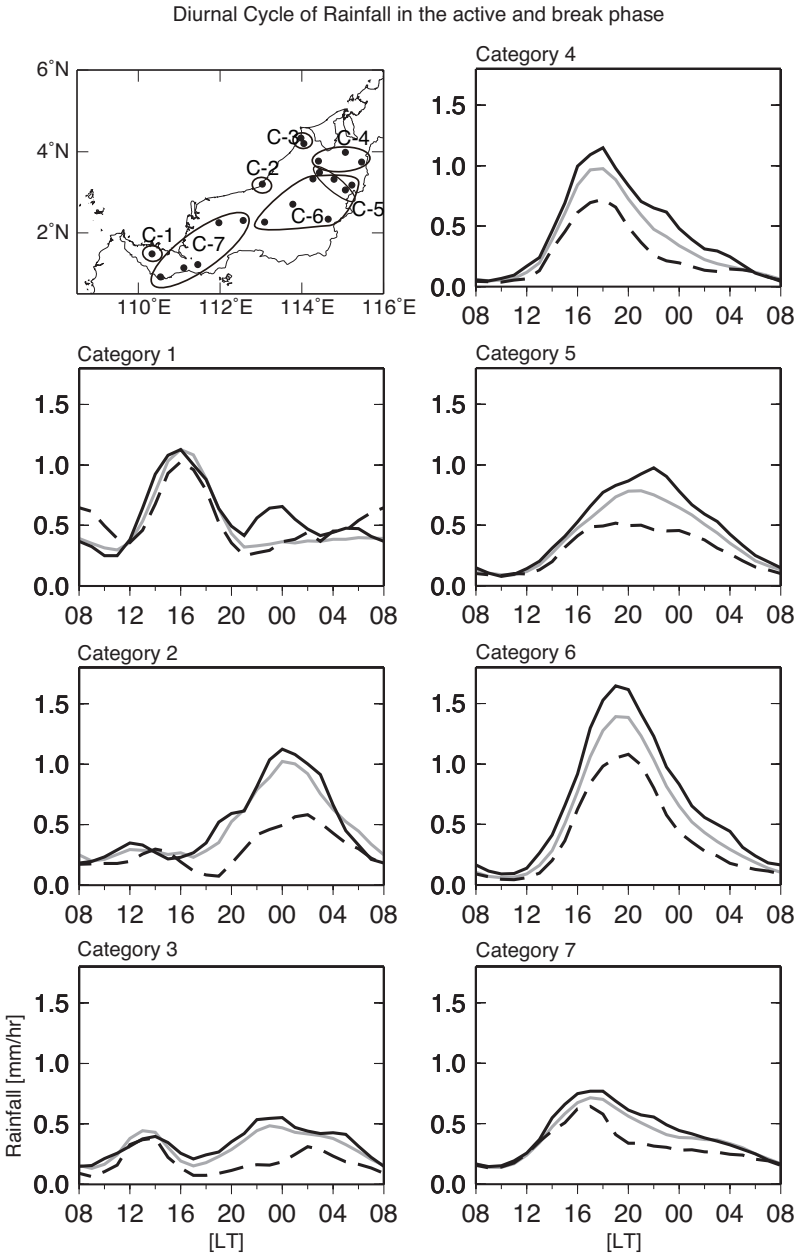

Figure 3.9. Composite of DCP based on gauge data, in both active and break phases for seven categories. Solid (dashed) line indicates active (break) phase precipitation in each category. Gray solid line indicates 5-yr mean DCP, as shown in Fig. 3.4.

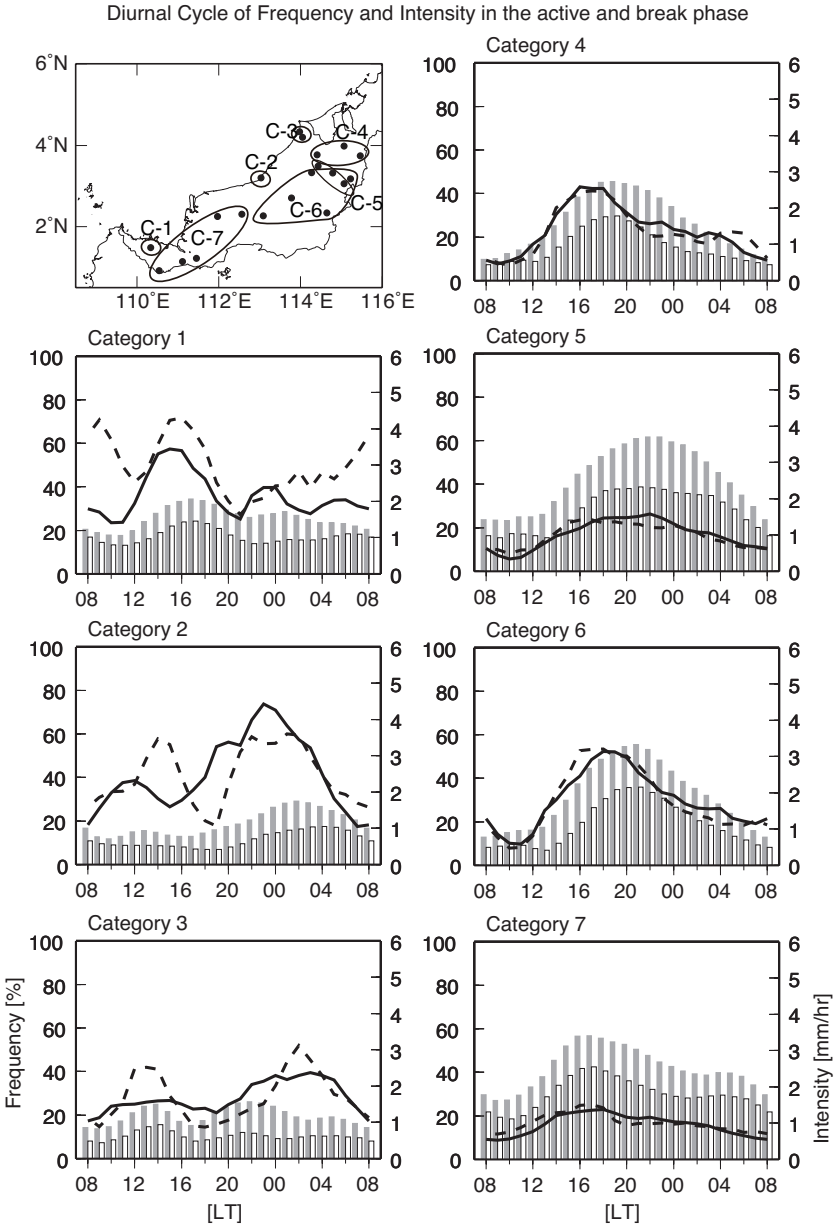

Figure 3.10. Composite of DC of frequency (%) and intensity (mm/hr) of precipitation for seven categories. Gray (white) bar indicates frequency of precipitation in active (break) phase with right axis, and solid (dashed) line indicates intensity of precipitation in active (break) phase with right axis, respectively.

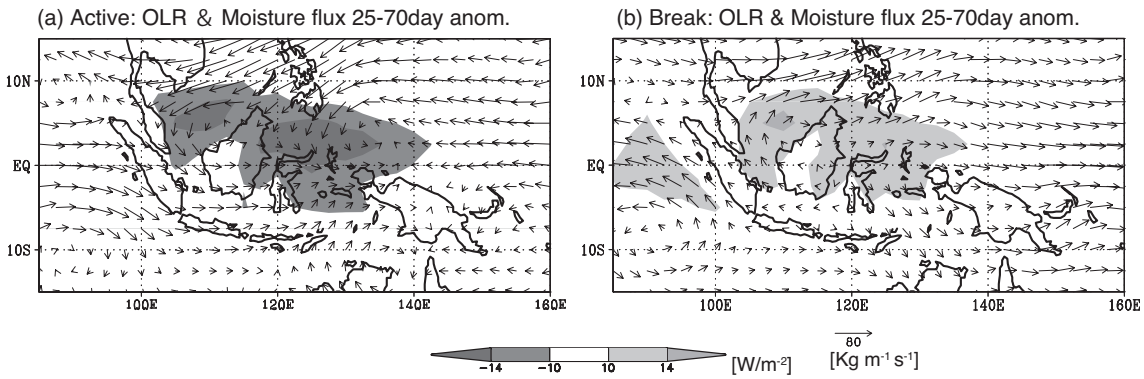

Figure 3.11. Spatial distribution of composite anomalies in 25 to 70-day band, based on OLR area-average time series. OLR (W/m^{-2}) and vertically integrated (from surface to 100 hPa) moisture flux vectors ($kg\ m^{-1}\ s^{-1}$) anomalies for (a) active, and (b) break phases.

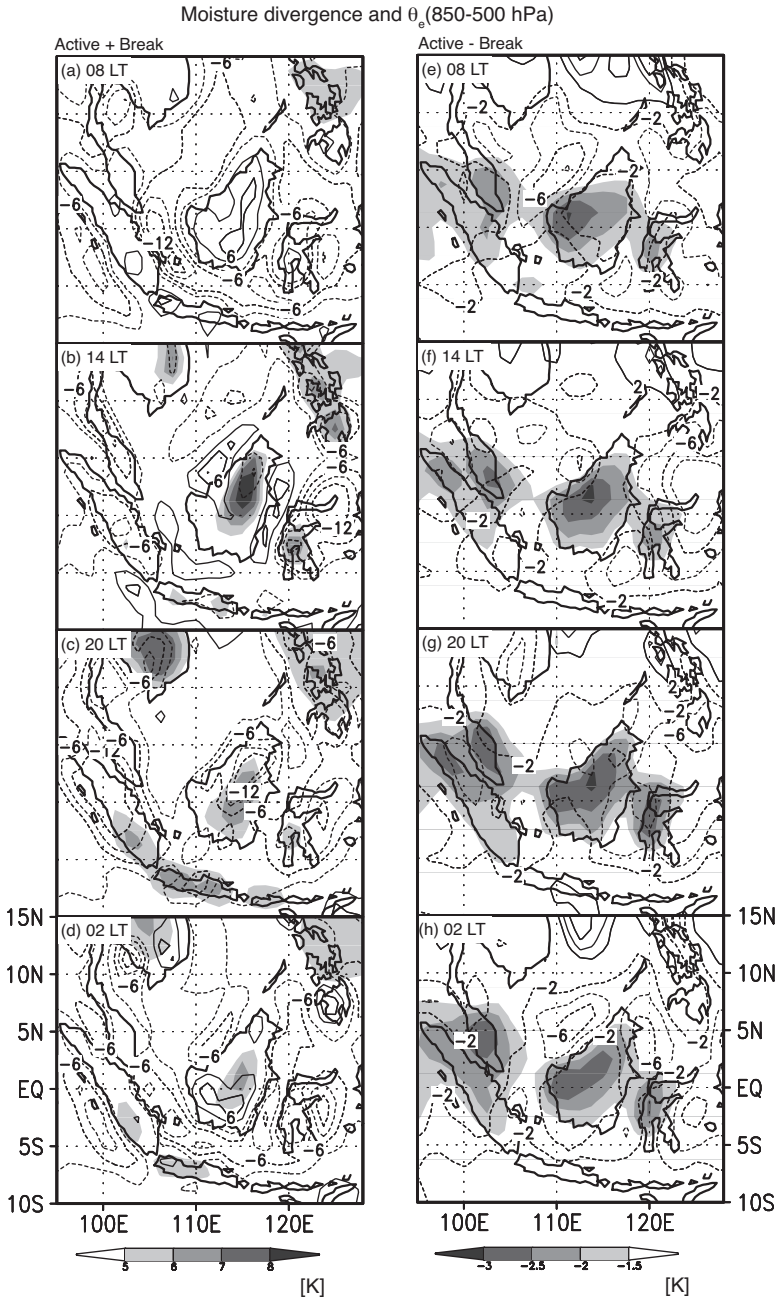

Figure 3.12. DC of vertically integrated (surface to 100 hPa) moisture divergence (contour), and atmospheric thermodynamic instability defined as the difference in equivalent potential temperature (θ_e) between 850 and 500 hPa [shaded; θ_e (850 hPa) − θ_e (500 hPa)], for (a) to (d) means of active and break phases. (e) to (h) As in (a) to (d), but for difference between peak active and break phases. For (a) to (d), contour interval for moisture divergence is −12.0, −9.0, −6.0, −3.0, 3.0 6.0, 9.0 and 12.0. For (e) to (h), this interval is −8.0, −6.0, −4.0, −2.0, 2.0, 4.0 6.0, and 8.0. Unit is 1×10^{-5} kg m^{-2} s^{-1}.

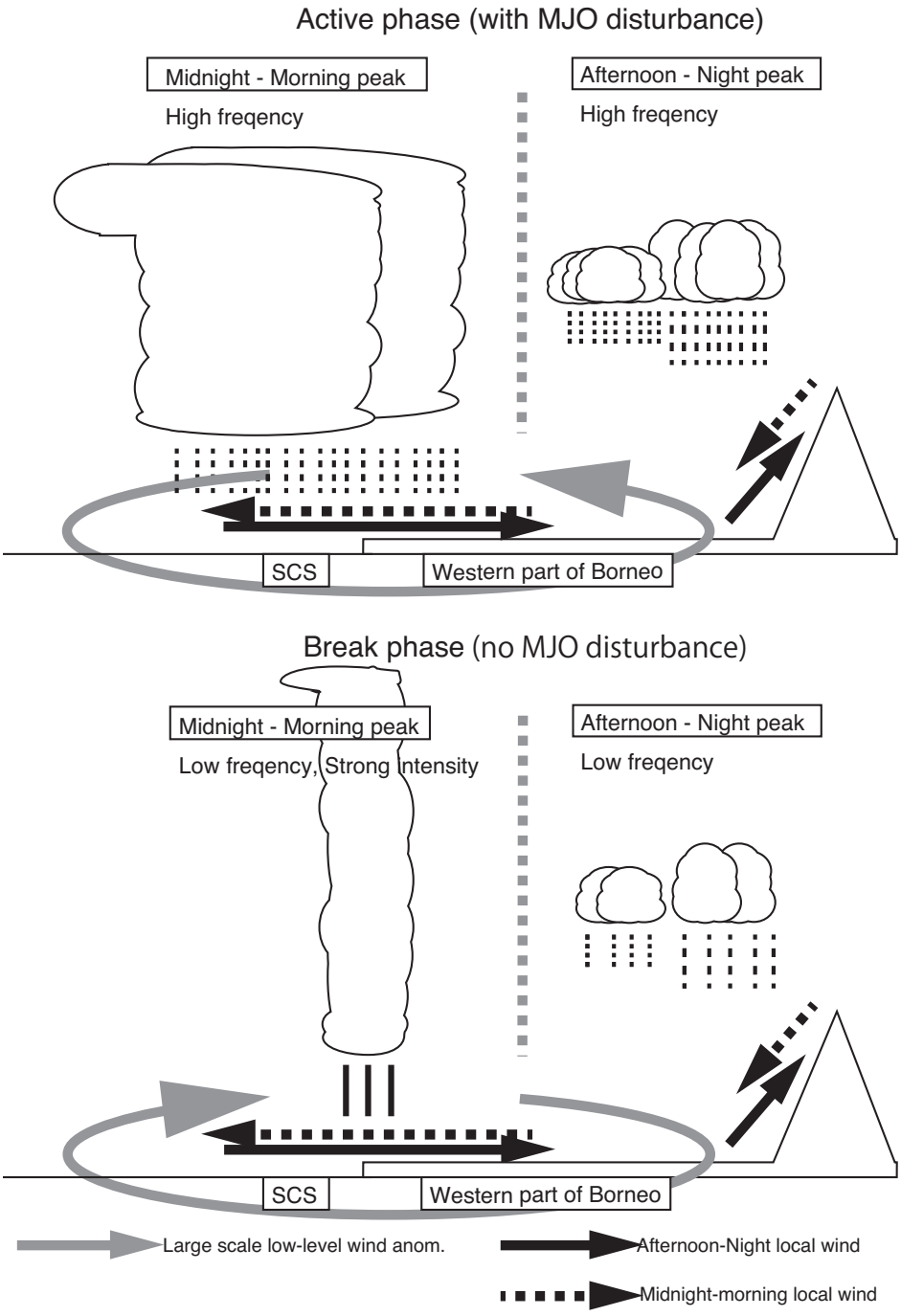

Figure 3.13. Diurnal schematics of precipitation and cloud systems over Sarawak – active phase (upper), and break phase (bottom). Gray arrows show large-scale, low-level circulation anomaly associated with MJO. Black solid (dashed) arrows show local circulation winds, which indicate land-sea breeze and mountain-valley circulations, from afternoon to night (midnight to morning).

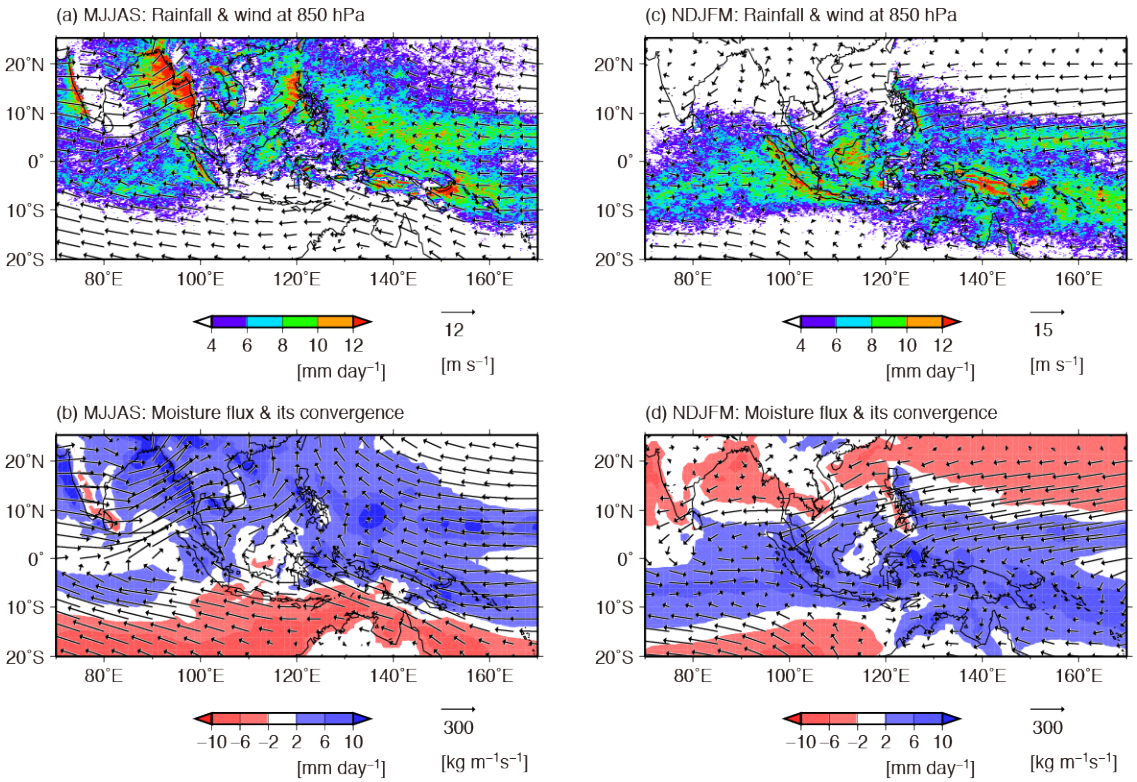

Figure 4.1. Climatological (1998–2012) mean distribution of (a) TRMM-PR precipitation (mm day^{-1}) (shaded areas) and wind vectors (m s^{-1}) at 850 hPa, and (b) vertically integrated moisture (from the surface to 100 hPa) flux vectors (kg m^{-1} s^{-1}) and its convergence (mm day^{-1}) (shaded areas) in boreal summer (MJJAS: May–September). (c) and (d) same as in (a) and (b), but in boreal winter (NDJFM: November–March).

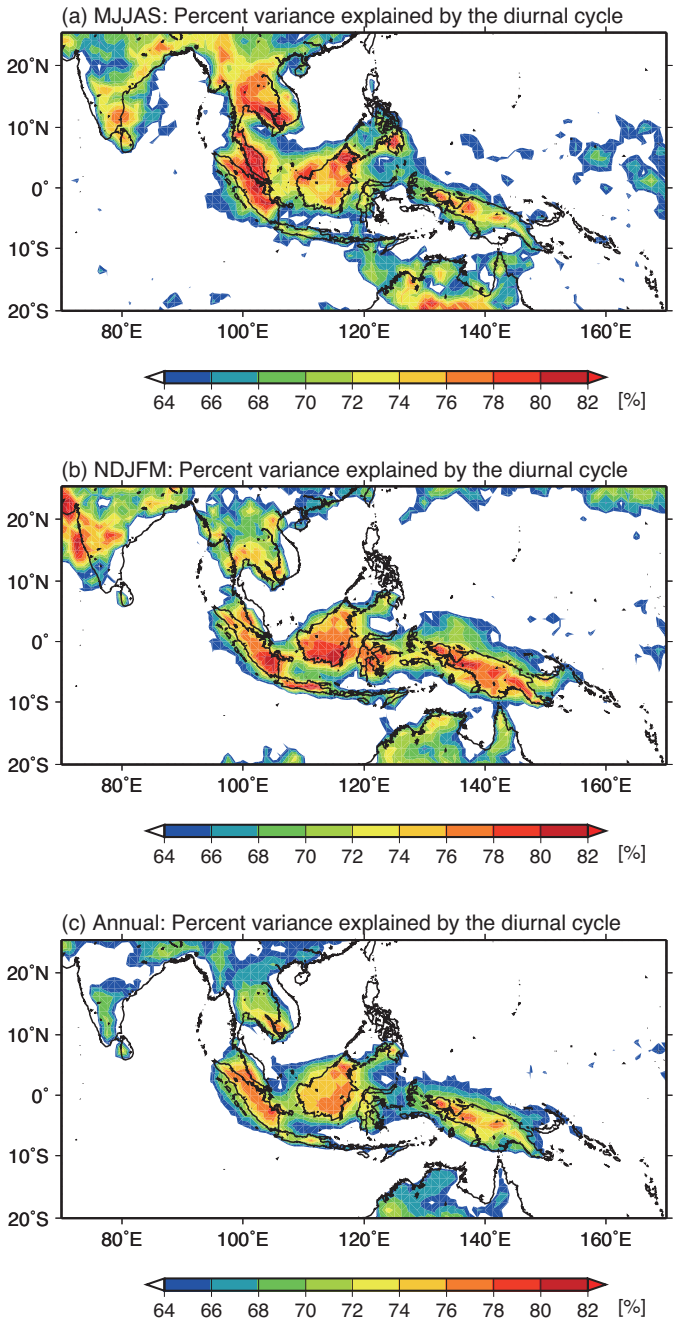

Figure 4.2. Distribution of the percentage (%) of the total variance explained by the diurnal cycle of precipitation from TRMM 3B42 precipitation in (a) MJJAS, (b) NDJFM and (c) annual mean.

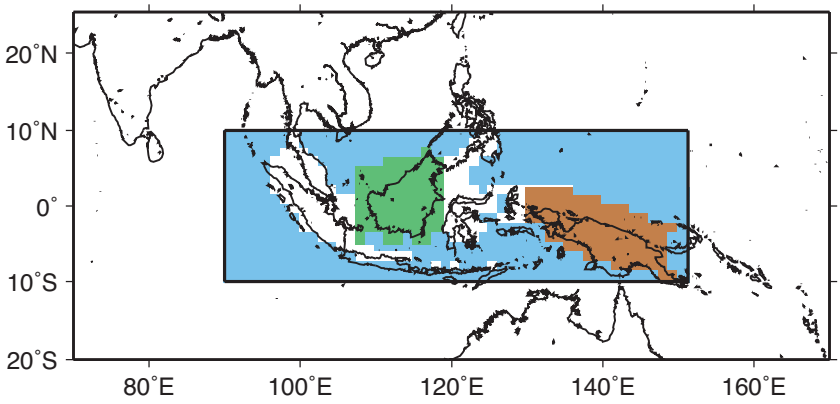

Figure 4.3. Three computational domains for examining the atmospheric hydrological water budget. These domains are defined using the annual mean (percentage) of the total variance explained by the diurnal precipitation cycle. The green and brown colors show Borneo (BO) and New Guinea (NG), respectively. Both regions are sub-divided into land (BOL and NGL) and coastal (BOC and NGC) regions. The blue shading shows the maritime continent ocean (MCO) region.

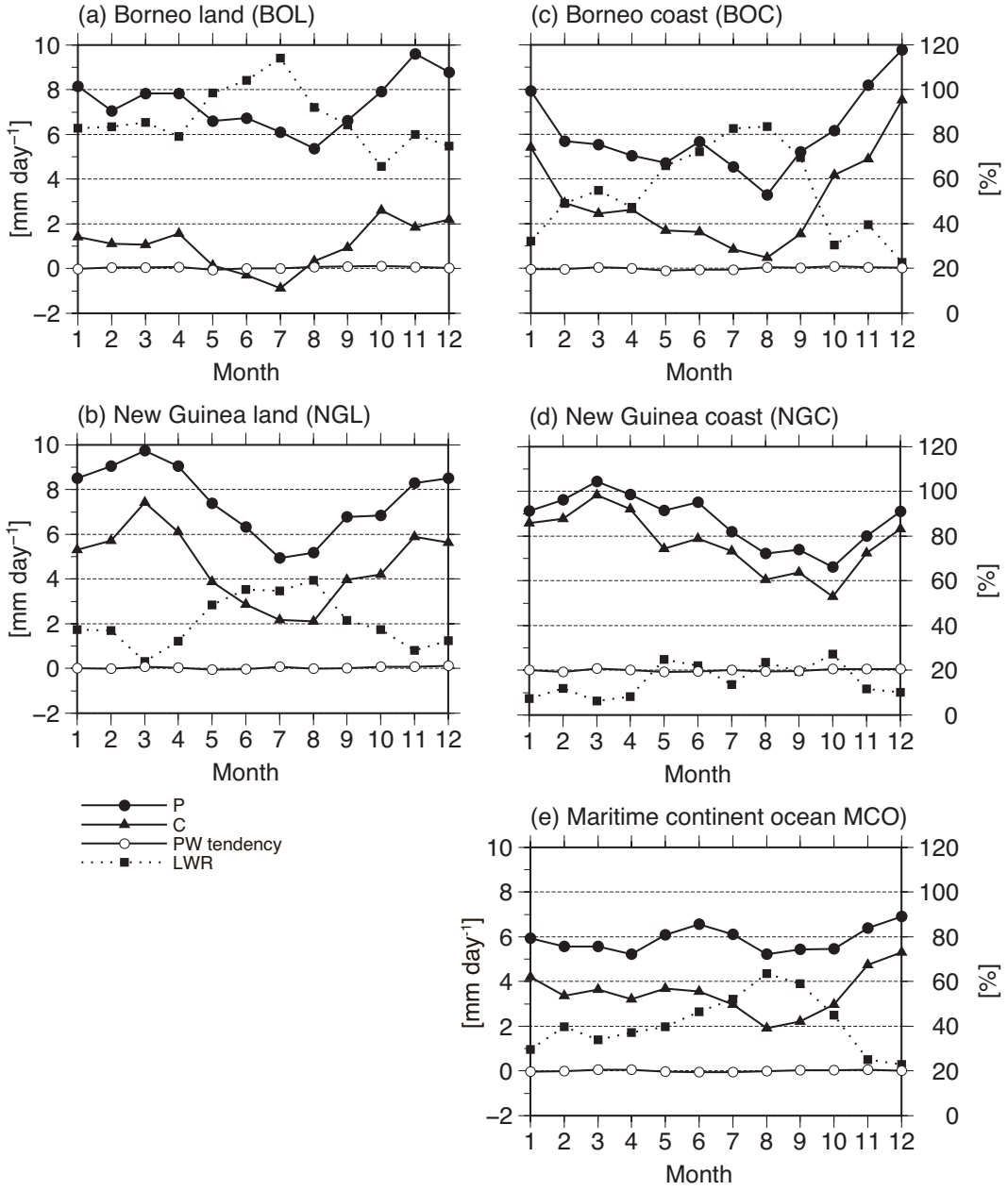

Figure 4.4. Climatological (1998–2012) annual precipitation (*P*) cycle, moisture flux convergence (*C*), temporal change in precipitable water content (PW) (mm day^{-1}), and the local water use ratio (LWR) (%) over the (a) BOL, (b) NGL, (c) BOC, (d) NGC, and (d) MOC.

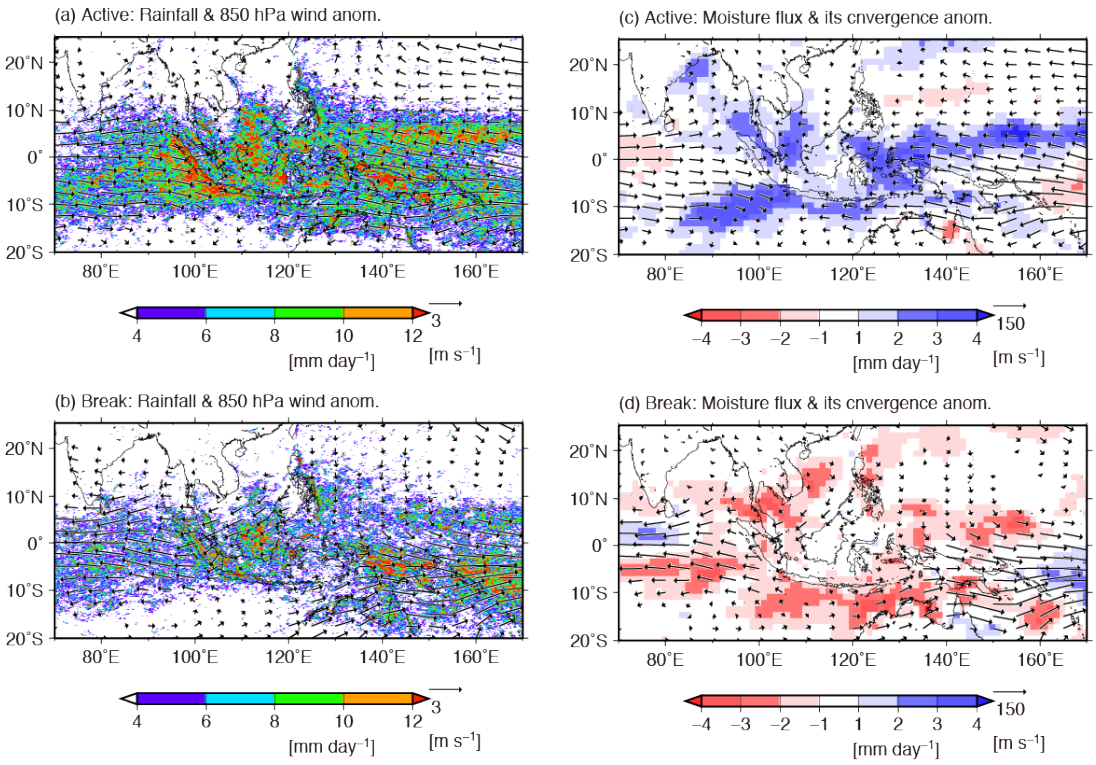

Figure 4.5. Composite of daily precipitation (mm day^{-1}) (shaded areas) and anomalies of wind vectors (m s^{-1}) at 850 hPa in the (a) active and (b) break phases. These anomalies are the difference from the boreal winter (NDJFM) mean. (c)–(d) same as in (a)–(b), but for anomalies of vertical integrated moisture flux vectors (kg m^{-1} s^{-1}) and convergence (mm day^{-1}) (shaded areas). Vectors and the moisture flux convergence are only plotted if significant at 95% confidence.

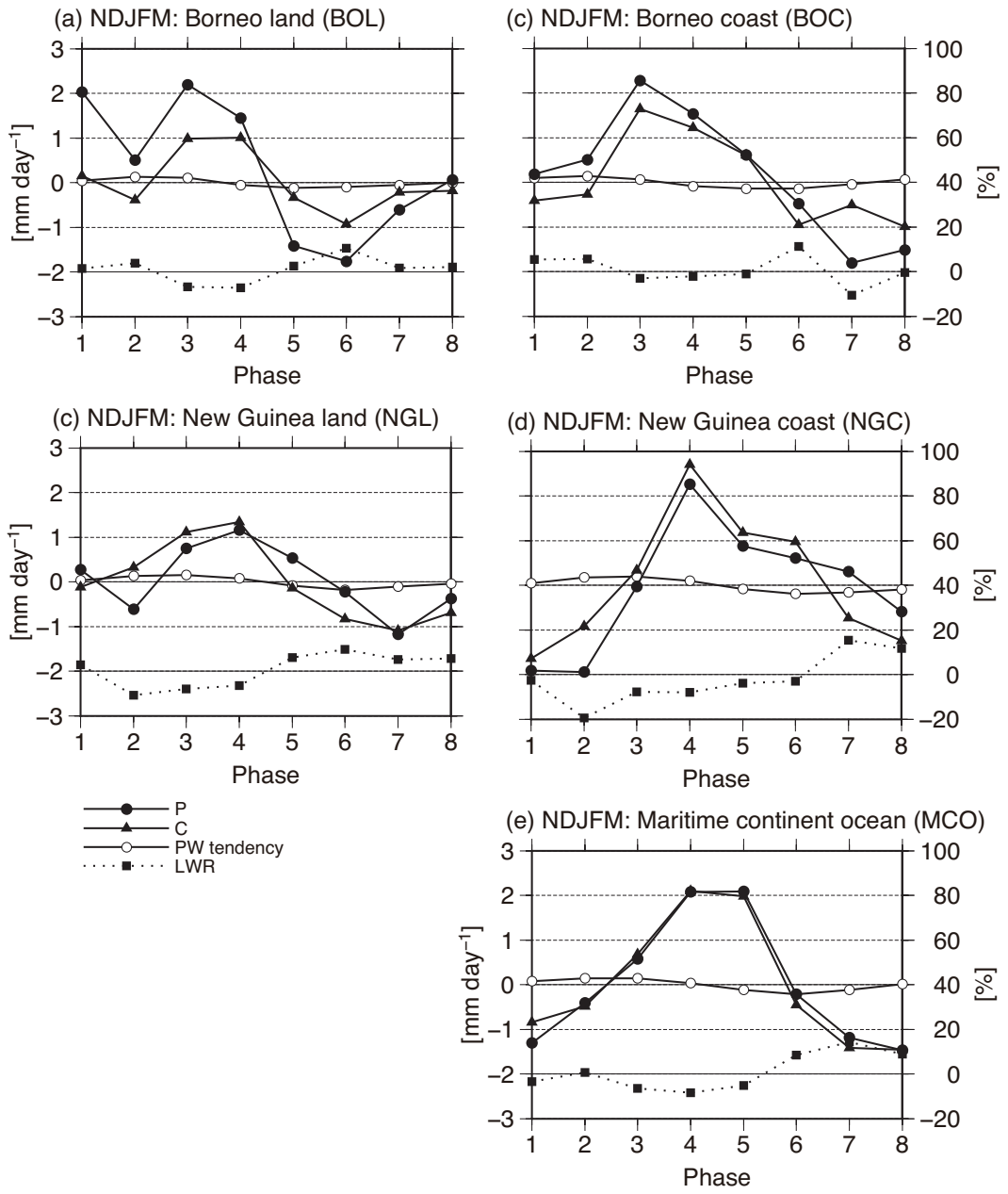

Figure 4.6. Composite of precipitation (*P*), moisture flux convergence (*C*), temporal change in precipitable water content (PW) (mm day^{-1}), and the local water use ratio (LWR) (%) anomalies during each MJO phases over: (a) BOL, (b) NGL, (c) BOC, (d) NGC, and (d) MCO. These anomalies indicate the difference from the seasonal mean (NDJFM).

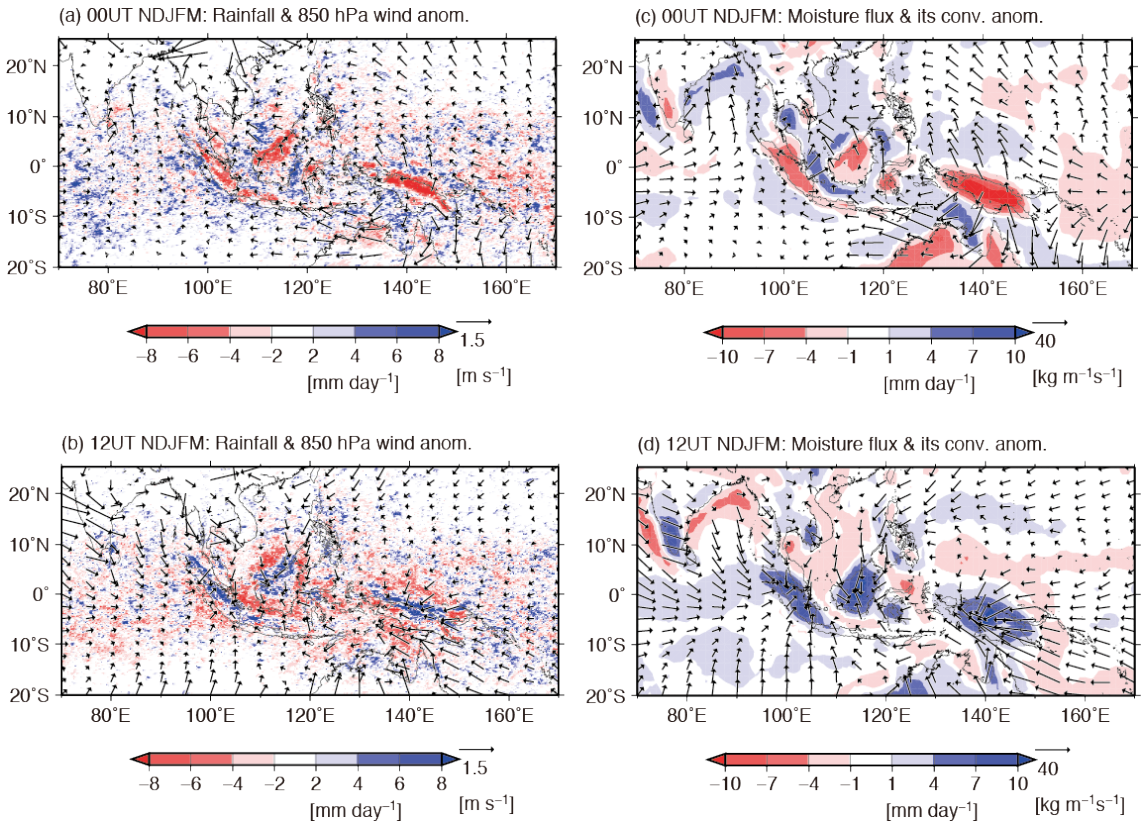

Figure 4.7. (a)–(b) Climatological (1998–2012) mean of TRMM-PR precipitation (mm day^{-1}) (shaded areas) and wind vectors (m s^{-1}) at 850 hPa at 0000 UTC and 1200 UTC in NDJFM. (c)–(d) same as in (a)–(b), but for vertically integrated moisture flux vectors (kg m^{-1} s^{-1}) and convergence (mm day^{-1}) (shaded areas). The daily mean at each grid point has been removed.

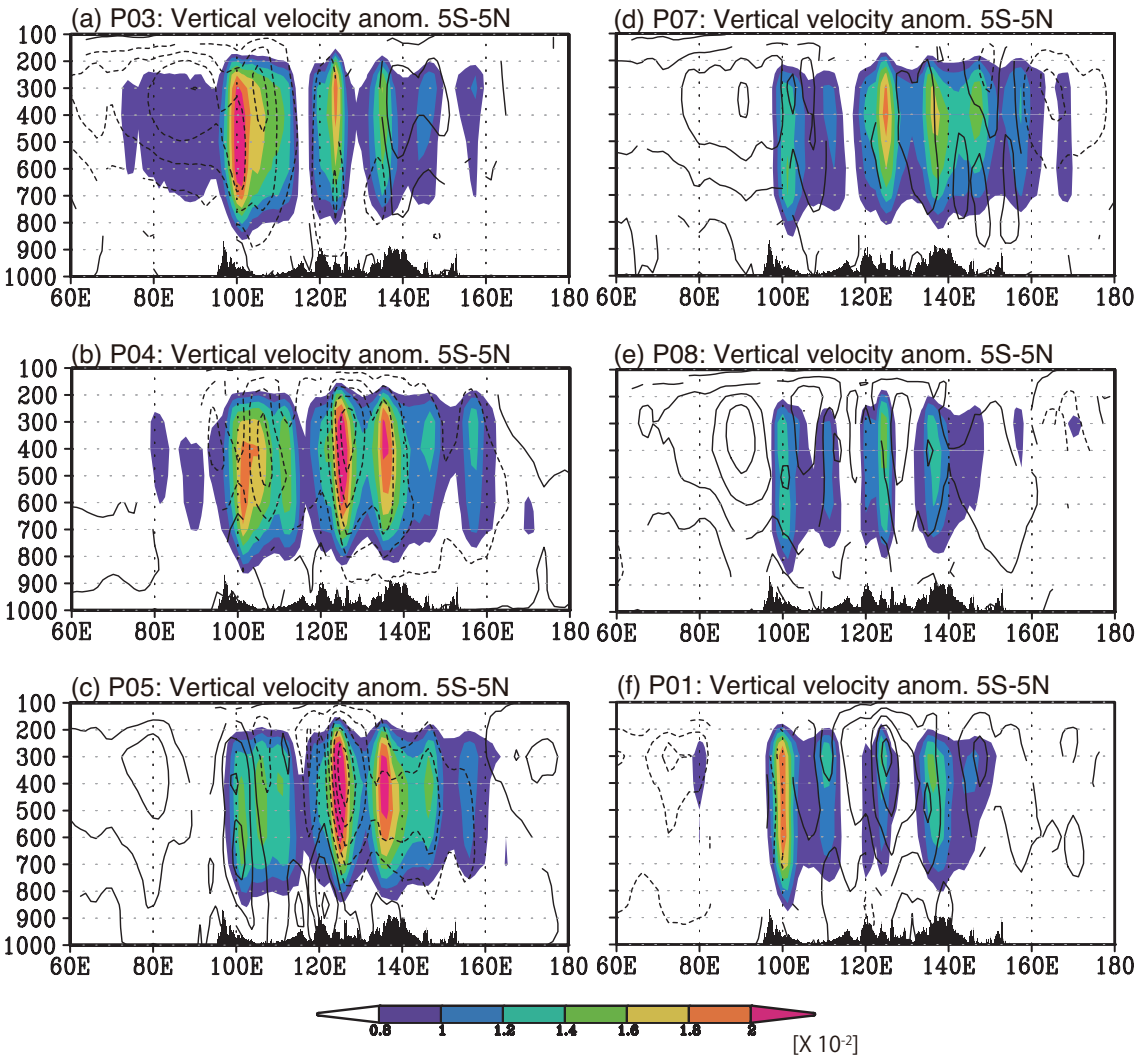

Figure 4.8. Composite vertical–longitude diagrams of vertical velocity anomalies (contours) and their diurnal variance (shaded areas) averaged between 5°S and 5°N in (a)–(c) peak active and (d)–(f) break phases. These anomalies show the difference from the seasonal mean (NDJFM). The black shading on the bottom of the figures denotes the topography. The solid (dashed) contours show positive (negative) values. The contour interval is 1×10^{-2} Pa s^{-1}, from −5 to 4×10^{-2} Pa s^{-1}. Contours and shading are only plotted if significant at 95% confidence.

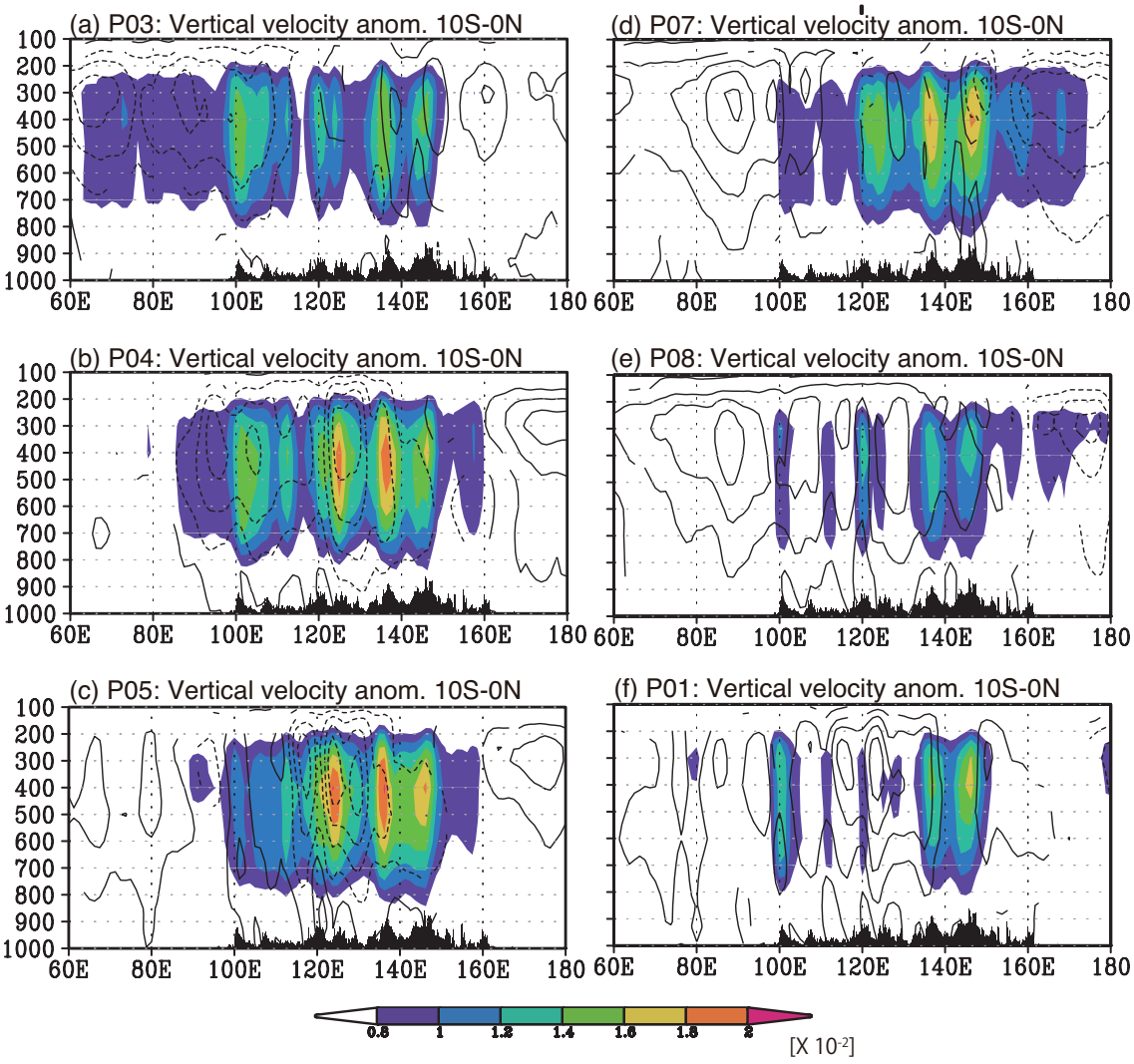

Figure 4.9. Same as Fig. 4.8, but averaged between 10°S and 0°N.

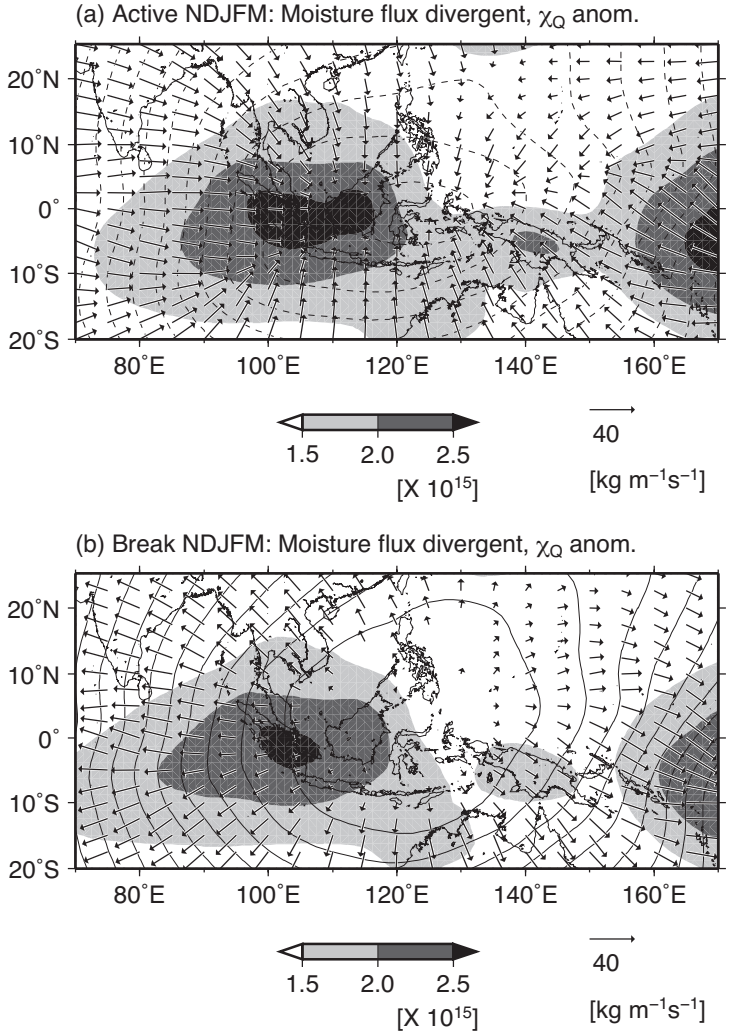

Figure 4.10. Composite anomalies of the velocity potential (kg s^{-1}) (contours) and divergent wind vectors (kg m^{-1} s^{-1}) of vertical integrated moisture fluxes in peak (a) active and (b) break phases. These anomalies show the difference from the seasonal mean (NDJFM). The shading also indicates the composite variance in the diurnal component of the velocity potential of integrated moisture fluxes between both phases. The solid (dashed) contours show positive (negative) values. The contour interval is 1 × 10^8 kg s^{-1}, from −1.2 to 1.3 × 10^8 kg s^{-1}.

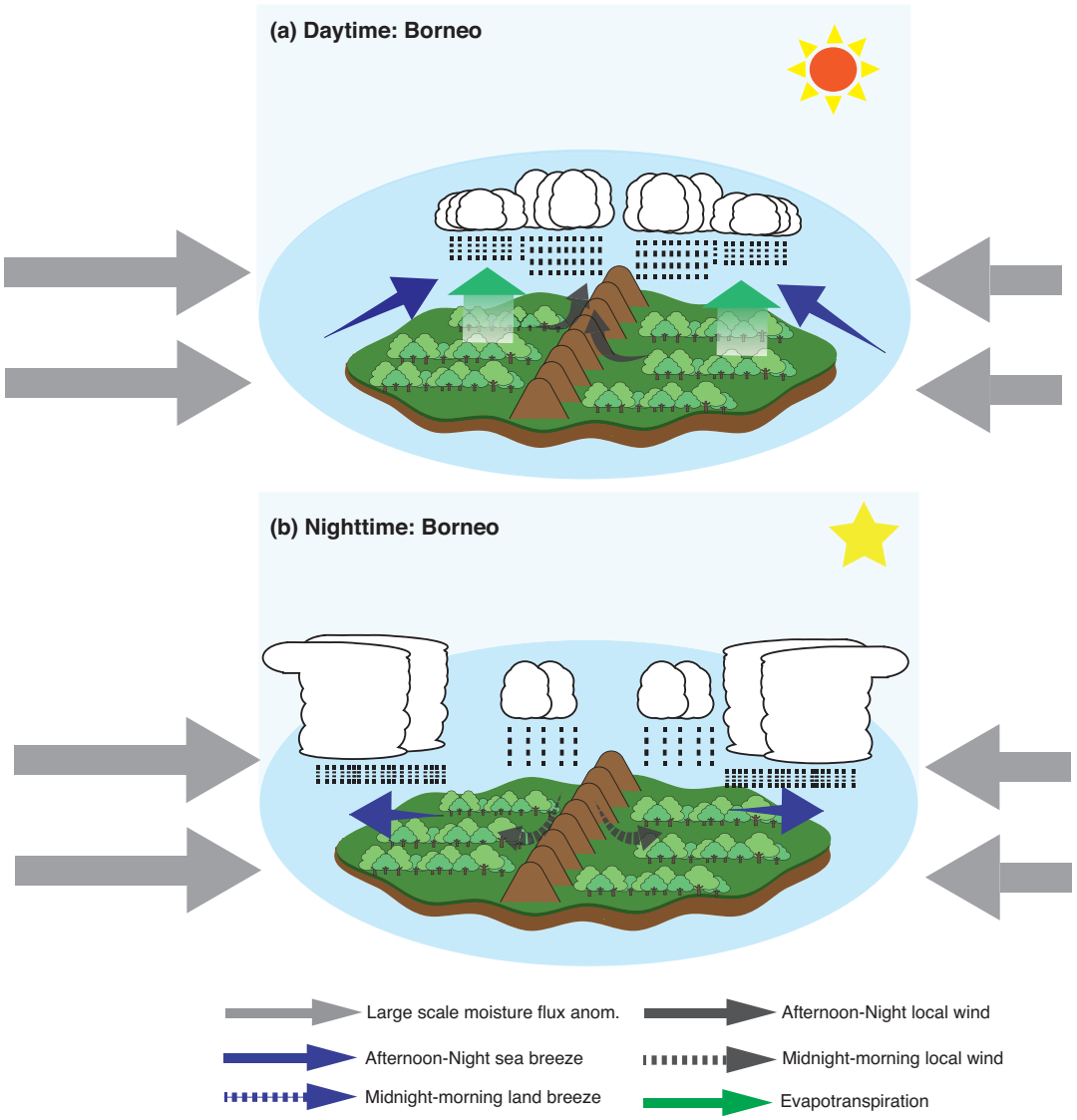

Figure 4.11. Schematics of atmospheric water cycles over Borneo: (top) daytime and (bottom) nighttime. Gray arrows show the large-scale vertical integrated moisture flux anomaly associated with the active phase of the MJO. Black solid (dashed) arrows show local circulation winds that indicate mountain–valley circulations from afternoon to night (midnight to morning). Blue solid (dashed) arrows show local circulation winds that indicate land–sea breeze from afternoon to night (midnight to morning). Green solid arrows show the evapotranspiration from the tropical rainforest.

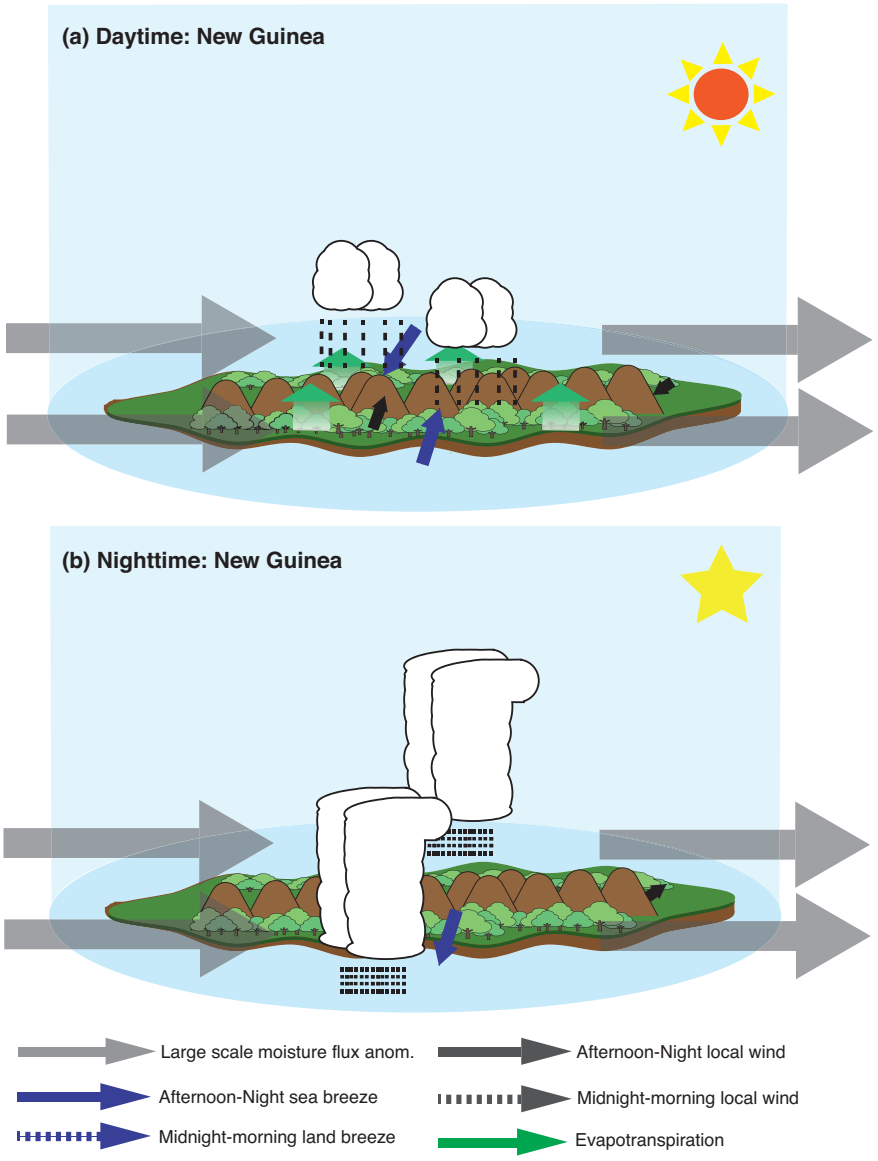

Figure 4.12. Same as Fig. 4.11, but for schematics of atmospheric water cycles over New Guinea.